Fish as major carbonate mud producers and missing components of the tropical carbonate factory

Chris T. Perry[a,1], Michael A. Salter[a], Alastair R. Harborne[b], Stephen F. Crowley[c], Howard L. Jelks[d], and Rod W. Wilson[b,1]

[a]School of Science and the Environment, Manchester Metropolitan University, Chester Street, Manchester M1 5GD, United Kingdom; [b]Biosciences, College of Life and Environmental Sciences, University of Exeter, Exeter EX4 4PS, United Kingdom; [c]Department of Earth and Ocean Sciences, University of Liverpool, 4 Brownlow Street, Liverpool L69 3GP, United Kingdom; and [d]US Geological Survey, 7920 North West 71st Street, Gainesville, FL 32653

Carbonate mud is a major constituent of recent marine carbonate sediments and of ancient limestones, which contain unique records of changes in ocean chemistry and climate shifts in the geological past. However, the origin of carbonate mud is controversial and often problematic to resolve. Here we show that tropical marine fish produce and excrete various forms of precipitated (nonskeletal) calcium carbonate from their guts ("low" and "high" Mg-calcite and aragonite), but that very fine-grained (mostly <2 μm) high Mg-calcite crystallites (i.e., >4 mole % $MgCO_3$) are their dominant excretory product. Crystallites from fish are morphologically diverse and species-specific, but all are unique relative to previously known biogenic and abiotic sources of carbonate within open marine systems. Using site specific fish biomass and carbonate excretion rate data we estimate that fish produce ~6.1 × 10^6 kg CaCO$_3$/year across the Bahamian archipelago, all as mud-grade (the <63 μm fraction) carbonate and thus as a potential sediment constituent. Estimated contributions from fish to total carbonate mud production average ~14% overall, and exceed 70% in specific habitats. Critically, we also document the widespread presence of these distinctive fish-derived carbonates in the finest sediment fractions from all habitat types in the Bahamas, demonstrating that these carbonates have direct relevance to contemporary carbonate sediment budgets. Fish thus represent a hitherto unrecognized but significant source of fine-grained carbonate sediment, the discovery of which has direct application to the conceptual ideas of how marine carbonate factories function both today and in the past.

marine teleost | fish intestine | carbonate production

Marine carbonates contain unique records of changes in ocean chemistry, biogeochemical cycling, and benthic and pelagic ecology (1), and therefore provide vital information on climate shifts in the geological past. A distinctive and often volumetrically important component of these sediments is carbonate mud (the <63 μm sediment fraction). However, the origins of both aragonitic and Mg-calcite carbonate muds remains a topic of long-standing debate (2, 3). Indeed, where attempts have been made to quantify sources of the fine sediment fraction a high proportion remains of unknown origin (e.g., up to 40% in Bahamian sediments and between 28 and 36% in Belize lagoon sediments) (4, 5). This problem arises in part because, with the exception of inorganic carbonate precipitation (e.g., the carbonate "whiting" controversy) (3, 6–8), the processes of carbonate mud production necessarily invoke the degradation of larger bioclasts (skeletal fragments of marine organisms) to produce mud-grade carbonate, and/or grain recrystallization to produce high Mg-calcite muds (9–11). Thus attempts to determine primary mud sources and production budgets are often hampered because of grain obliteration. The mineralogical composition of the mud fraction of modern tropical carbonate sediment is also very variable between settings: in some environments the finest sediment fractions are predominantly aragonite (12, 13), but high Mg-calcite can account for in excess of 40% of the mud fraction in many settings (14–16). Ultimately variable admixtures of both arago-

nite and Mg-calcite mud-grade carbonate occur and thus budgetary considerations need to accommodate production from a range of potential sources. This issue has important geo-environmental implications because carbonate muds are major constituents of limestones and are volumetrically important in most modern shallow marine carbonate environments (17). Furthermore, the presence of Mg-calcite muds in marine carbonates is considered critical to preserving primary sediment textures and fabrics (15), thus influencing sediment porosity and permeability which are of critical importance to fluid flow in limestone sequences. Mud production in ancient limestones has proven particularly perplexing because evidence is often lacking for the presence of species that are regarded as key modern mud producers (especially the calcareous green algae) (18).

Recent observations of carbonate crystals growing within, and being continually excreted from, the intestines of temperate fish species (19) lead us to speculate that such crystals could represent a hitherto unrecognized source of mud-grade carbonate in shallow tropical marine environments. In these shallow marine environments carbonate production rates are typically high and preservation potential is good because of high carbonate saturation states in the overlying waters. The process by which fish precipitate carbonate crystals within their guts has been documented in some detail (19–22) and occurs within the teleosts (bony fish) that dominate the marine fish fauna. Briefly, precipitation occurs as a by-product of the osmoregulatory requirement of teleosts to continuously drink Ca- and Mg-rich seawater. Subsequent intestinal bicarbonate secretion generates exceptionally high concentrations of HCO_3^- (50–100 mM) and very high pH values (up to 9.2) which leads to the alkaline precipitation of calcium and magnesium within ingested seawater as insoluble carbonates along the intestine (19–24; Fig. 1). Carbonate precipitation is believed to occur within the mucus that is secreted along the entire length of the intestinal lumen (21, 23, 24), and carbonates are subsequently excreted within mucus-coated pellets. Following their excretion the rapid degradation of the organic mucus matrix is assumed to release inorganic crystals into the water column (19). Whilst the physiological processes driving fish carbonate production are thus increasingly well understood, the morphological characteristics of such carbonates and their sedimentological significance have never been considered.

Results and Discussion

In order to study the morphological and compositional characteristics of carbonates produced by tropical marine fish, carbo-
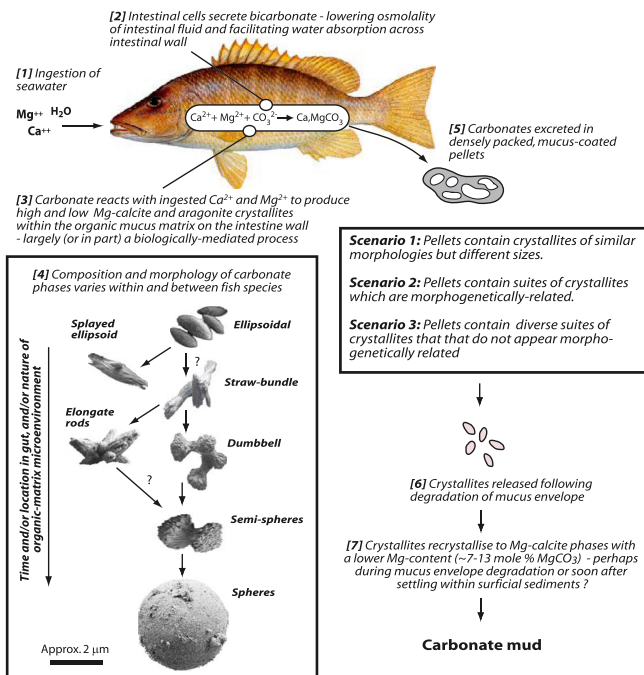
Fig. 1. Fish carbonate production and precipitation products. Schematic diagram illustrating the processes associated with carbonate precipitation within the intestines of fish and the dominant crystallite morphologies identified in this study to be produced by tropical fish species.

nate samples were obtained from 11 common fish species (see *SI Appendix*) collected from shallow water sites on the Eleuthera Bank, Bahamas (*SI Appendix: Fig. S1*). This area was selected for study as it combines warm, shallow waters that are supersaturated with respect to CaCO$_3$, and comprises a range of typical carbonate platform sedimentary environments. The mucus-coated pellets excreted from fish guts that contain the carbonate precipitates vary in shape and size with fish species (*SI Appendix: Fig. S2*), but subsequent degradation of the organic mucus phase in the laboratory, through dilute hypochlorite treatments (see *SI Appendix*), releases inorganic carbonate pellets up to 2 mm in size. Each pellet comprises huge numbers of individual crystallites and polycrystalline precipitates (in most cases estimated at >10^6 per pellet; *SI Appendix: Fig. S2*), along with an amorphous "matrix" of finer (<0.25 μm) carbonate. When subjected to even gentle ultrasonic agitation, rapid pellet disaggregation occurs, resulting in the release of large volumes of fine-grained crystallites (*SI Appendix: Fig. S3*).

Different fish species produce different types of pellet (in terms of size, shape, and density of precipitate packing) that consist of crystallites and polycrystalline aggregates of varying size and morphology (Fig. 1 and *SI Appendix: Figs. S4–S14*), although most are <2 μm in size. Despite the differences between species, four particularly common morphologies occur from the range of fish examined: ellipsoidal; straw bundle-shaped; dumbbell-shaped; and spheroidal (Fig. 2 *A–D*). In addition, several less common morphologies occur including: (*i*) semi-spherical polycrystalline aggregates (Fig. 2*E*); (*ii*) polycrystalline aggregates that are rod-like (Fig. 2*F*), or form intertwined crosses; and (*iii*) "splayed ellipsoids" (Fig. 2*G*). These crystallite morphologies are highly distinctive and fundamentally differ from those associated with all known biogenic and abiotic sources of carbonate within tropical marine carbonate systems, including the basic crystal structures that build the skeletons of common tropical carbonate sediment producing species (10, 11). This observation alone has major significance from the perspective of establishing the origins of marine carbonate muds.
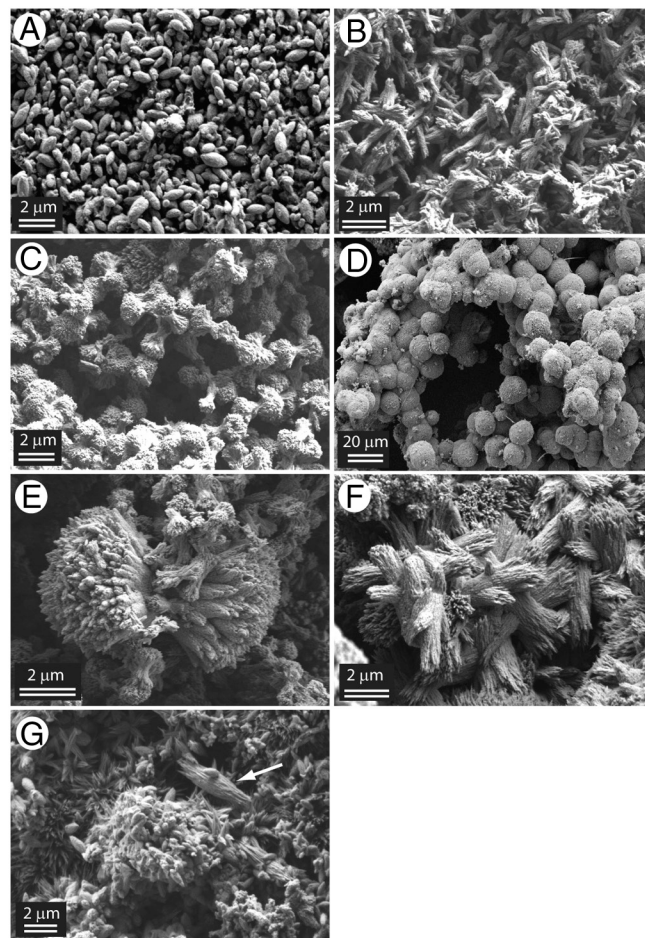

Fig. 2. Common morphologies of tropical fish-produced carbonate precipitates. (A) Type 1—Ellipsoidal crystallites (size range: <0.25 to 3 μm long); (B) Type 2—Straw-bundle crystallites (size range: 1–3 μm long); (C) Type 3 —Polycrystalline dumbbell-shaped aggregates (size range: typically 1–3 μm long, but large examples to ~10–15 μm also occur); (D) Type 4—Polycrystalline spheroidal aggregates (size range: <10 to 30 μm diameter). Occur both as discrete spheres and as multilobate aggregations of spheres; (E) Large polycrystalline aggregates with a semisphere morphology (size range: ~5 to ~30 μm diameter); (F) Elongate rod-like crystallites which often occur as intergrown bundles of crystallites (size range: 2–3 μm long); (G) Splayed ellipsoidal crystallites (size range ~2 μm long and narrow towards their terminal points).

High Mg-calcite (i.e., >4 mole% MgCO$_3$) is the dominant carbonate phase precipitated by these tropical fish species. This finding is confirmed in X-ray diffraction (XRD) analysis of bulk samples from a range of the fish examined (*SI Appendix: Fig. S15 A and B*), and in energy dispersion X-ray microanalysis (EDX) of the dominant crystallite morphologies produced by each fish species (Fig. 3 and *SI Appendix: Figs. S4–S14*). XRD analyses also indicates that some fish species precipitate "low" (i.e., <4 mole% MgCO$_3$) Mg-calcite phases along with small volumes (typically less than a few %) of aragonite (*SI Appendix: Fig.S15 A and B*). Of particular interest is that recently excreted samples (collected with 24 h) from all fish species predominantly comprise "high" Mg-calcite phases, with average MgCO$_3$ contents ranging from 18–39 mol% dependant on species (Fig. 3). These Mg levels are considerably higher than those from other carbonate producers at comparable latitudes (Fig. 3), and are also well above the average MgCO$_3$ content of both tropical marine carbonate sediments (13.5 mol% MgCO$_3$) and naturally occurring marine inorganic Mg-calcite cements (11.9 mole% MgCO$_3$) (26). However, as we discuss below, our preliminary
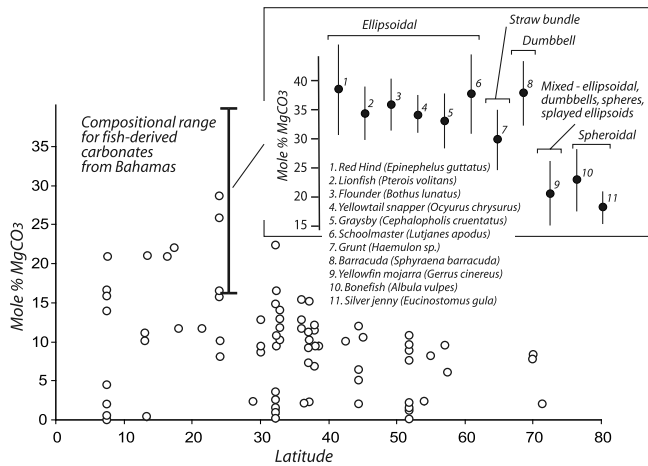
Fig. 3. Comparison of mole% MgCO$_3$ of fish-derived carbonates and skeletal Mg-calcite producing benthic organisms. Latitudinal data for skeletal benthic organisms (white circles) from Chave (25). Fish-derived data from Eleuthera at 25° N plotted as average MgCO$_3$ contents ($+/-$ 1 s.d.) (black circles) based on EDX analysis ($n = 50$ analyses per fish) of dominant crystallite morphologies observed in each species. Samples are grouped based on the dominant crystal morphology associated with each fish species.

data indicate that recrystallization of fish carbonates to a lower Mg-calcite state seems to occur subsequent to their excretion in the natural marine environment (a key point in relation to the preservation potential of fish carbonates).

A crude relationship is observed between crystal form and mole fraction of MgCO$_3$. Samples with the highest average MgCO$_3$ contents (means ranging from 33.7 to 39.6 mol% MgCO$_3$) being dominated by small (1–2 μm) ellipsoidal and dumbbell morphology crystallites, while samples with lower MgCO$_3$ contents (means range from 18.6 to 23.1 mol % MgCO$_3$) are dominated by larger (10–20 μm) spheroids (Fig. 3). We speculate that this variability may reflect a progressive reduction in the MgCO$_3$ content of crystallites as they grow larger and/or as the crystallite forms evolve during growth. These ideas remain to be tested.

The unusual occurrence of the observed crystal forms and the precipitation of crystals outside normal stability ranges of Mg-calcite, raises a number of questions about controls on carbonate precipitation inside the guts of fish and how stable these carbonate forms are once excreted. To our knowledge such crystallite forms have not previously been described within open marine systems, the only similar crystals having been described from natural marine environments deriving from intertidal microbial mats, where dumbbell-, rod- and sphere-type morphologies have been identified as bacterially-mediated precipitates (27). It is also the case that numerous in vitro studies have grown crystals with very similar morphologies through both synthetic inorganic and organically-induced precipitation, but that those showing the greatest similarity to fish carbonates were also bacterially mediated (28, 29). This observation raises some fundamental questions about the potential role of microbial activity in mediating carbonate precipitation and growth within the intestines of marine teleost fish, even though antibiotic treatment was previously shown to have no obvious effect, at least quantitatively, on total gut carbonate production in one species of marine fish (20). However, it is also the case that fish intestinal fluids are hypo-saline with respect to normal seawater (approximately one third of ambient seawater) and this, alongside observed differences in pH, Ca^{2+}, Mg^{2+}, HCO$_3^-$, and CO$_3^{2-}$ levels longitudinally within the intestines of temperate fish species (23), indicates that these carbonates are formed under conditions with a distinctive chemistry compared to other marine calcifiers.

While both the high MgCO$_3$ content and the crystallite morphologies observed distinguish these fish carbonates from

those previously documented in tropical marine environments, two significant questions arise that are pertinent to the wider significance of fish crystal production in the tropics. First, how much total carbonate do tropical fish produce? And second, how significant is this carbonate in the context of carbonate mud production? To address the first question, we measured fish body mass and carbonate excretion rates in 11 different Bahamas fish species (see *SI Appendix*). Average production rates vary between species and range from ~10 × g CaCO$_3$/kg fish/year in barracuda (*Sphyraena barracuda*) to >80 × g CaCO$_3$/kg fish/year in schoolmaster (*Lutjanes apodus*). However, production rates are strongly dependent upon body mass (scaling similarly to metabolic rate—see *SI Appendix: Fig. S16* for further details), such that smaller fish produce relatively more carbonate on a mass-specific basis (see *SI Appendix*). By combining this production rate data with habitat-specific fish biomass data from sites around the Bahamas and with the measured area of each habitat, it is then possible to scale our data to consider fish carbonate production rates at regional spatial scales (see *SI Appendix*). On this basis we estimate that fish produce ~6.1 × 10^6 kg CaCO$_3$ across the Bahamian archipelago each year (an area of ~111,577 km^2). Major contributions from fish derive from gorgonian-hardground habitats (~2.3 × 10^6 kg CaCO$_3$ year^{-1}) and medium-density seagrass beds (~1.2 × 10^6 kg CaCO$_3$ year^{-1}) reflecting the large areas these habitats cover, but the highest rates per unit area occur in reef habitats and within mangrove-fringed embayments, reflecting much higher densities of fish biomass (Fig. 4). It is important to point out, however, that these figures are likely to be highly conservative because: (*i*) the habitat mapping does not delineate individual patch reefs across the sand and seagrass dominated platform environments, but which are focal points of high fish biomass in these areas; and (*ii*) because our calculations are based primarily on fish biomass data from areas that are outside marine reserves (i.e., our surveyed areas are significantly reduced by fishing). Within reef and gorgonian-hardground habitats, for example, fish-derived carbonate production increases by 202% and 139% respectively, when biomass data from only those sites inside marine reserves are used, and even higher rates would be expected under historical "pristine" ecological conditions (30).

To address the question about contributions to mud production, we compared our measures of fish carbonate production against regional estimates of mud production for different platform top habitats (see *SI Appendix*). On this basis, we estimate
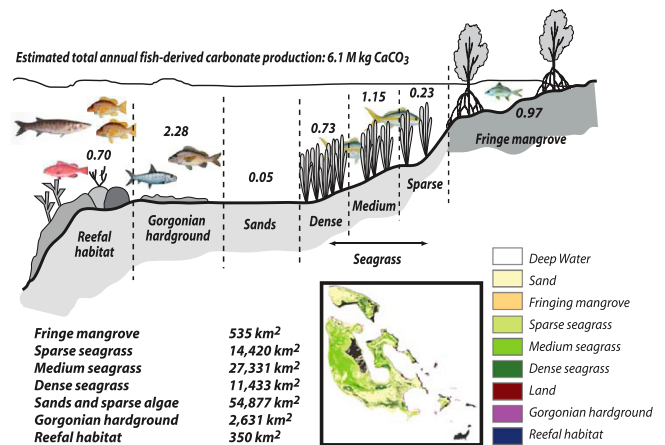

Fig. 4. Estimates of fish carbonate production across the Bahamian archipelago. Summary diagram showing estimated volumes of carbonate (millions kg CaCO$_3$/yr) produced in different habitats across the Bahamas. Production volume estimates are based on measured fish body mass and carbonate excretion data, combined with known habitat-specific fish biomass data for the region (see *SI Appendix: Methods*).

that fish contribute an average ~14% to total estimated carbonate mud production across the Bahamian archipelago each year, although contributions vary markedly between habitats. Relative contributions are, for example, very low (<1%) across the platform top seagrass and algal meadow habitats where mud production derives predominantly from calcareous epiphytes, calcareous algal breakdown, and/or inorganic ("whiting") precipitation. In contrast, the contribution from fish is much higher in hardground (~25%) and in fringing mangrove habitats (~70%), reflecting the greater fish biomass in these environments. Contributions to mud production in reef habitats average ~2.6%, but are much higher (~6%) if equivalent fish biomass data from marine reserves is used.

The archipelago-wide estimates from the Great Bahama Bank suggest that fish produce carbonate at sufficient rates to influence shallow marine carbonate sediment budgets and consequently their role in carbonate mud production requires serious consideration. Whilst the mud fraction on the Great Bahama Bank is predominantly aragonite, derived mainly from algal breakdown or carbonate "whitings" (see refs. 2, 7, 8 for discussions), between 10 and 32% is high Mg-calcite (15) and thus fish provide a viable explanation for the origin of a major portion of this type of sediment. Furthermore, the Mg-calcite content of the mud fraction of sediments from many other sites is even higher: in southern Belize ~45% (16); in Florida 50–75% (14); and in northern Belize 70–90% (9)—the proportion increasing in the <20 μm fraction. It is therefore highly significant that analysis of the finest grain-size fractions from sediment samples recovered from sites across the Eleuthera Bank (see *SI Appendix*) all contain carbonate crystallites that are morphologically identical to those collected from fish in our experiments (Fig. 5 and *SI Appendix: Fig. S17*). This critical observation provides clear evidence that fish carbonates do accumulate in modern sedimentary environments and do not simply dissolve immediately postexcretion, despite their high $MgCO_3$ content at the point of release (31, 32). Preliminary data also indicate that the fish crystals observed within surface sediments, despite remaining morphologically similar to the freshly excreted carbonates (Fig. 5 and *SI Appendix: Fig. S17*), have already recrystallized to more stable high Mg-calcite forms (~7–13 mole% $MgCO_3$). Thus recrystallized fish carbonates are comparable in their chemical composition to many other biogenic high Mg-calcite grains (26), indicating that they should have good preservation potential within the adjacent sedimentary environments.

It is also the case that fish carbonates represent a unique direct source of high Mg-calcite mud-grade carbonate i.e., a source whose production is not dependent upon postmortem grain disaggregation or bioclast breakdown and recrystallization, as necessarily invoked to explain the production of Mg-calcite mud from other sources (9–11)—see ref. 33 for possible submarine precipitation sources. Further work is clearly required to elucidate the pathways from the release of fish carbonate crystals to their deposition and early diagenesis within marine sediments, and to quantify fish crystal abundances in the finest (<20 μm) fractions of carbonate platform and shelf sediments. However, the data presented clearly demonstrate that fish carbonates represent a primary source of high Mg-calcite mud-grade carbonate, and that these carbonates are produced in sufficient quantities to have direct relevance to tropical carbonate sediment budgets within the Holocene (last 12,000 years). Furthermore, given that bony marine fish probably evolved as early as the Ordovician (488–444 Million years) (34) and that "modern" reef fish assemblages have existed since at least the Eocene (56–34 Million years) (35) the implications for addressing some of the major unknowns about the provenance of carbonate muds in the geologic record are considerable.
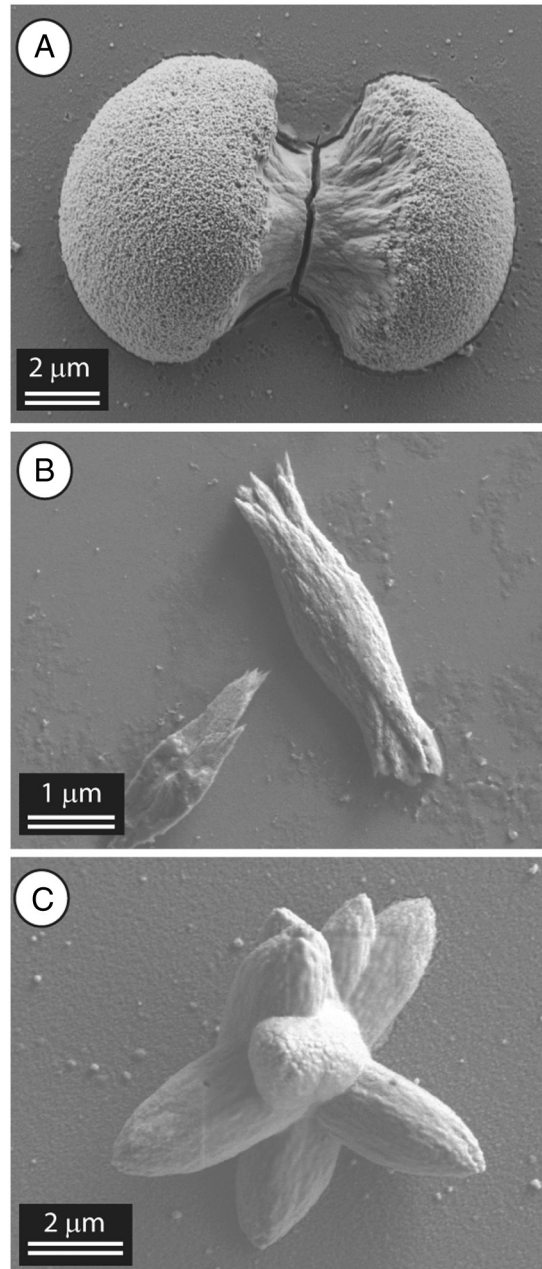

Fig. 5. Crystallites in the fine-sediment fractions from a range of modern environments across the Eleuthera Bank, Bahamas. (*A*) Discrete dumbbell morphology crystallites from reefal environments (15 m water depth); (*B*) Splayed ellipsoidal morphology crystallites from reefal environments (15 m water depth); (*C*) Cluster of ellipsoidal morphology crystallites from shallow mangrove-fringed coastal inlet site

Materials and Methods

Data. We measured rates of carbonate production and examined the morphological and chemical composition of carbonate precipitates in 11 species of tropical fish (*SI Appendix: Table S1*) collected from the shallow water environments around Eleuthera, The Bahamas (24° 50′N, 76° 20′ W). Following collection fish were held in holding tanks provided with flow-through filtered seawater without feeding for 48 h prior to collections starting (see *SI Appendix*). Mucus pellets produced by the fish were collected at 24 h intervals and subjected to replicate distilled water rinses and treatments in sequential 3 h treatments with excess sodium hypochlorite (5.25% by mass; commercial bleach) in order to disaggregate the organic component of the mucus pellets from the carbonate crystals. Samples were then filtered and dried prior to morphological and chemical analysis (see *SI Appendix*), with a subset of the cleaned inorganic crystals used to determine carbonate production rates per unit of time.

Analysis. We used Scanning Electron Microscopy (SEM), EDX, and XRD to examine the morphological and chemical characteristics of the carbonate crystallites produced by each fish species. Carbonate production rates per unit of time were determined by titration using the double titration method (see *SI Appendix*). In order to scale measured fish carbonate production rate data to habitat scales across The Bahamas we integrated recent Geographical Information Systems (GIS)-derived data on the areal extent of different habitat types from The Bahamas with habitat-specific fish biomass data, supplemented with data on cryptic species densities in comparable marine habitats from sites in St. Croix, US Virgin Islands. Rates of mud-grade carbonate production per unit area by fish, as measured in this study, were compared against published rates of production from other known carbonate mud producers in The Bahamas, including production by calcareous algae, seagrass epiphytes and carbonate whitings.

1. Maloof AC, et al. (2009) Sedimentary iron cycling and the origin and preservation of magnetization in platform carbonate muds, Andros Island, Bahamas. *Earth Planet Sci Lett* 259:581–598.
2. Shinn EA, Steinen RP, Lidz BH, Swart PK (1989) Whitings, a sedimentologic dilemma. *J Sed Pet* 59:147–161.
3. Morse JW, Arvidson RS, Lüttge A (2007) Calcium carbonate formation and dissolution. *Chem Rev* 107:342–381.
4. Stieglitz RD (1972) Scanning electron microscopy of the fine fraction of recent carbonate sediments from Bimini, Bahamas. *J Sed Pet* 42:411–426.
5. Gischler E, Zingeler D (2002) The origin of carbonate mud in isolated carbonate platforms of Belize, Central America. *Int J Earth Sci* 91:1054–1070.
6. Milliman JD, Freile D, Steinen RP, Wilber R.J (1993) Great Bahama Bank aragonitic muds: mostly inorganically precipitated, mostly exported. *J Sed Pet* 63:589–595.
7. Broecker WS, Takahashi AC (1966) Calcium carbonate precipitation of the Bahama Banks. *J Geophys Res* 71:1575–1602.
8. Robbins LL, Tao Y, Evans CA (1997) Temporal and spatial distribution of whitings on the Great Bahama Bank and a new lime mud budget. *Geology* 25:947–950.
9. Reid RP, Macintyre IG, Post JE (1992) Micritized skeletal grains in northern Belize lagoon: a major source of Mg-calcite mud. *J Sed Pet* 62:145–156.
10. Debenay J-P, André J-P, Lesourd M (1999) Production of lime mud by breakdown of foraminiferal tests. *Mar Geol* 157:159–170.
11. Reid RP, Macintyre IG (1998) Carbonate recrystallization in shallow marine environments: a widespread diagenetic process forming micritized grains. *J Sed Res* 68:928–946.
12. Hoskin CM (1968) Magnesium and strontium in mud fraction of recent carbonate sediment, Alacrán reef, Mexico. *Am Assoc Petr Geol B* 52:2170–2177.
13. Adjas A, Masse J-P, Montaggioni LF (1990) Fine-grained carbonates in nearly closed reef environments: Mataiva and Takapoto atolls, Central Pacific Ocean. *Sediment Geol* 67:115–132.
14. Andrews JE, Christidis S, Dennis PF (1997) Assessing mineralogical and geochemical heterogeneity in the sub 63 micon size fraction of Holocene lime muds. *J Sed Res* 67:531–535.
15. Husseini SI, Matthews RK (1972) Distribution of high-magnesium calcite in lime muds of the Great Bahama Bank: diagenetic implications. *J Sed Pet* 42:179–182.
16. Matthews RK (1966) Genesis of recent lime mud in southern British Honduras. *J Sed Pet* 36:428–454.
17. Purdy EG, Gischler E (2003) The Belize margin revisited: 1. Holocene marine facies. *Int J Earth Sci* 92:532–551.
18. Wright VP, Churns L (2007) *Controls on carbonate platform and reef development*, eds J Lukasik and JA Simo (SEPM Special Publ, Tulsa, OK), pp 47–54.
19. Wilson RW, et al. (2009) Contribution of fish to the marine inorganic carbon cycle. *Science* 323:359–362.
20. Walsh PJ, Blackwelder P, Gill KA, Danulat E, Mommsen TP (1991) Carbonate deposits in marine fish intestines : a new source of biomineralization. *Limnol Oceanogr* 36:1227–1232.
21. Wilson, RW, Wilson JM, Grosell M (2002) Intestinal bicarbonate secretion by marine teleost fish—why and how? *Biochim Biophys Acta* 1566:182–193.
22. Wilson RW, Gilmour KM, Henry RP, Wood CM (1996) Intestinal base excretion in the seawater-adapted rainbow trout: a role in acid-base balance? *J Exp Biol* 199:2331–2343.
23. Marshall WS, Grosell M (2005) *The physiology of fishes*, eds DH Evans and JB Claiborne (CRC Press, Boca Raton), pp 177–230.
24. Humbert W, Kirsch R, Simonneaux V (1986) Is mucus involved in biomineralization? Study of the intestinal mucus of the sea-water eel *Anguilla anguilla* L. *Cell Tissue Res* 245:599–604.
25. Chave KE (1954) Aspects of biogeochemistry of magnesium 1. Calcareous marine organisms. *J Geology* 65:266–283.
26. Garrels R, Wollast R (1978) Equilibrium criteria for two-component solids reacting with fixed composition in an aqueous phase—example: the magnesian calcites, Discussion. *Am J Sci* 278:1469–1474.
27. Chafetz HS, Buczynski C (1992) Bacterial induced lithification of microbial mats. *Palaios* 7:277–293.
28. González-Muñoz MT, et al. (2008) Ca-Mg kutnahorite and struvite production by *Idiomarina* strains at modern seawater salinities. *Chemosphere* 72:465–472.
29. Rivadeneya MA, Martín-Algarra A, Sánchez-Navas A, Martín-Ramos D (2006) Carbonate and phosphate precipitation by *Chromohalobacter marismortui*. *Geomicrobiol J* 23:1–13.
30. Knowlton N, Jackson JBC (2008) Shifting baselines, local impacts and global change on coral reefs. *PLoS Biol* 6:0215–0220.
31. Morse JW, Mackenzie FT (1990) *Geochemistry of sedimentary carbonates* (Elsevier, New York).
32. Morse JW, Gledhill DK, Millero FJ (2003) CaCO$_3$ precipitation kinetics in the waters from the Grand Bahama Bank: implication for the relationship between bank hydro-chemistry and whitings. *Geochim Cosmochim Acta* 67:2819–2826.
33. Macintyre IG, Aronson RB (2006) Lithified and unlithified Mg-calcite precipitates in tropical reef environments. *J Sed Res* 76:81–90.
34. Zhu M, et al. (2009) The oldest articulated osteichthyan reveals mosaic gnathostome characters. *Nature* 458:469–474.
35. Bellwood DR (1996) The Eocene fishes of Monte Bolca: the earliest coral reef fish assemblage. *Coral Reefs* 15:11–19.

GEOLOGY

PHYSIOLOGY

Supplementary Information: Perry et al. Fish carbonates

Fish collections and carbonate sampling. Fish species used in this study (Table S1) were collected from the shallow water carbonate platform environments around Eleuthera, The Bahamas (24° 50'N, 76° 20' W; Fig. S1). Sampling took place during November and December 2009 when sea surface temperatures were ~25 - 27 ˚C (i.e., around the mid-point of the annual regional sea surface temperature range of ~23 to ~30 ˚C). All fish species were collected from either nearshore areas close to Cape Eleuthera Institute (CEI) (in and around the nearshore creeks and inlets) or from sites adjacent to patch reefs on the open platform top. Fish were obtained using a variety of techniques including seine netting and hook and line. Captured fish were immediately returned to the aquaculture facility of the CEI and held in a range of stock tanks (60, 400 or 1400 litres) of suitable dimensions for the different size categories of fish (2 g to 13 kg). Tanks were all supplied with one-pass flow-through seawater with an average salinity of 36.6 ± 0.2 (n=10) and temperature of 25.8 ± 0.4 ˚C (n=15). The sea water supplied to experimental tanks was filtered to 5 μm.

Common name	Latin name	Functional group	Production Rate Data	Body Size Range	Precipitate morphological data
Schoolmaster	*Lutjanes apodus*	Piscivore-Invertivore	Yes	4.6 - 322 g	Yes
Yellowtail snapper	*Ocyurus chrysurus*	Piscivore-Invertivore	Yes	13.4 - 946 g	Yes
Grunt	*Haemulon sp.*	Macroinvertivore	Yes	101 g	Yes
Graysby	*Cephalopholis cruentatus*	Piscivore-Invertivore	Yes	58 - 185 g	Yes
Red Hind	*Epinephelus guttatus*	Piscivore-Invertivore	Yes	205 g	Yes
Yellowfin mojarra	*Gerrus cinereus*	Macroinvertivore	Yes	143 – 202 g	Yes
Silver Jenny	*Eucinostomus gula*	Invertivore	No	20 – 30 g	Yes
Great Barracuda	*Sphyraena barracuda*	Predator	Yes	41- 11,364 g	Yes
Bonefish	*Albula vulpes*	Invertivore	Yes	759 - 1506 g	Yes
Lionfish	*Pterois volitans*	Piscivore-Invertivore	Yes	25 - 381 g	Yes
Flounder	*Bothus lunatus*	Piscivore-Invertivore	No	81 g	Yes
Mullet	*Mugil sp.*	Detritivore-Planktivore-Invertivore	Yes	2 - 4 g	No

Supplementary Table 1. Fish collected in the present study and used to calculate carbonate excretion rates and for the examination of crystallite morphologies and compositions. Functional groups after Randall [34] and fishbase.org [35].
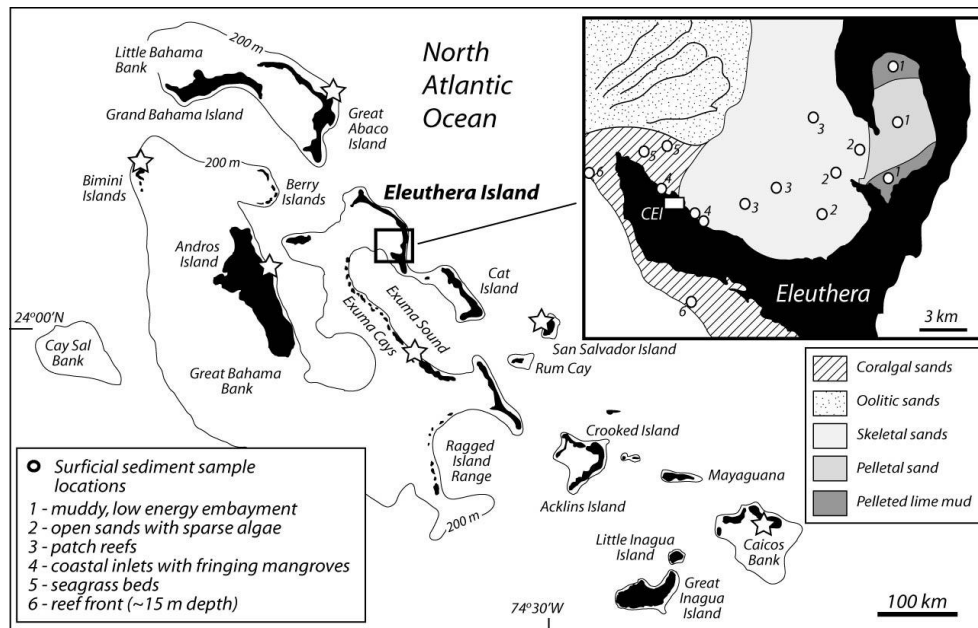
Supplementary Figure 1. Map showing regional location of study area in the Bahamas and (inset) the southern end of Eleuthera were the study was conducted. White stars on main map are locations of the fish census studies on which the fish biomass modelling aspects of this paper are based (from[36]). White-filled circles in inset map are sites where surficial sediment samples were collected for preliminary investigations into the occurrence of fish carbonates in the sediment record. Surficial sedimentary facies on Eleuthera are after Dravis [37].

Following collection from the wild, fish were held for at least 2 days without feeding prior to experiments to allow clearance of any previously eaten food from the gut. This avoided any potential for contamination of carbonates produced endogenously within the fish intestine with exogenous sources of carbonate that the fish may have previously ingested. Where possible, samples were collected from fish from a range of body sizes within the same species, although this was to some extent dictated by fish capture success. Starvation is known to reduce metabolic rate in all animals, including fish, and so the carbonate excretion rates determined under non-fed conditions will tend to under estimate the gross production rate by marine fish intestines [19,22]. After 48 hours without food, fish were moved from stock tanks to experimental aquaria fed by running, filtered (5 μm) seawater. Fish were held either individually or in small groups of similar sized fish within a given species. In species that tended to graze on material at the bottom, tanks were fitted with a false mesh floor to prevent fish from re-ingesting excreted carbonate pellets. Because carbonate pellets (i.e. aggregated crystals wrapped in mucus) are denser than seawater, they quickly settle on the true base of each tank, and so were collected every 24 hours from the bottom of each aquaria using a 10 ml plastic Pasteur pipette and transferred to 50 ml centrifuge tubes. Immediately following collection, samples were rinsed in distilled water to

remove extraneous seawater salts (3 sequential washes). This was followed by two sequential 3 hour treatments with excess sodium hypochlorite (5.25 % w/w; commercial bleach) to disaggregate the organic component of the mucus pellets from the carbonate crystals (Fig. S2). Following the hypochlorite cleaning process, inorganic crystal aggregates were allowed to settle, the overlying hypochlorite solution was gently siphoned off, and the remaining crystals rinsed three times in distilled water to remove all traces of hypochlorite. This bleaching treatment has been shown to have no discernible effect on carbonate mineralogy or grain texture [38]. Following these treatments the residual carbonates were flushed with deionised water and filtered onto 1.6 μm glass microfibre filters (Fisherbrand MF100) and then over-dried (40 ˚C for ~24 hours). After drying, filter papers were allowed to cool and then placed in air tight vials for subsequent analysis. A significant proportion of the carbonate material collected on the filter papers could be manually liberated with gentle agitation, and thus to avoid further excessive wetting and drying processes, these samples were prepared for Scanning Electron Microscopy (SEM), Energy-dispersion X-ray (EDX) and X-ray diffraction (XRD) analysis.

Analysis of fish carbonate samples. SEM and EDX analysis was undertaken using a Zeiss Supra 40VP FEG-SEM fitted with an Oxford Instruments ISIS energy dispersive analysis system. For morphological analysis of pellets and crystallites, samples were prepared both as loose grain mounts onto carbon coated SEM tabs (Fig. S3), or onto SEM stubs that had been covered with a thin veneer of silver epoxy. Both sets of samples produced good images under low vacuum conditions, avoiding the need for either gold or carbon coating. Samples were examined under an operating voltage of 2 kV and a working distance of 5-7 mm. Disaggregated samples were pipetted directly onto small silicon plates, previously mounted on SEM stubs, and the fluid allowed to evaporate in a low temperature (40˚C) oven. These samples again produced good images under low vacuum, avoiding the need for either gold or carbon coating. Following detailed SEM observations of crystallite morphologies (see Figs. S4-14), samples were also analysed using EDX to determine the composition of the dominant crystallite forms associated within each fish species. Mole % $MgCO_3$ was calculated for each of 50 individual analyses run on the dominant crystal morphologies previously identified in each species. For EDX analysis samples were examined under an operating voltage of 15 kV, with a working distance of 15 mm and an aperture setting of 120 microns. Count times ranged from 15 to 60 Lsecs with no quantitative differences in resultant analytical traces under shorter counts.
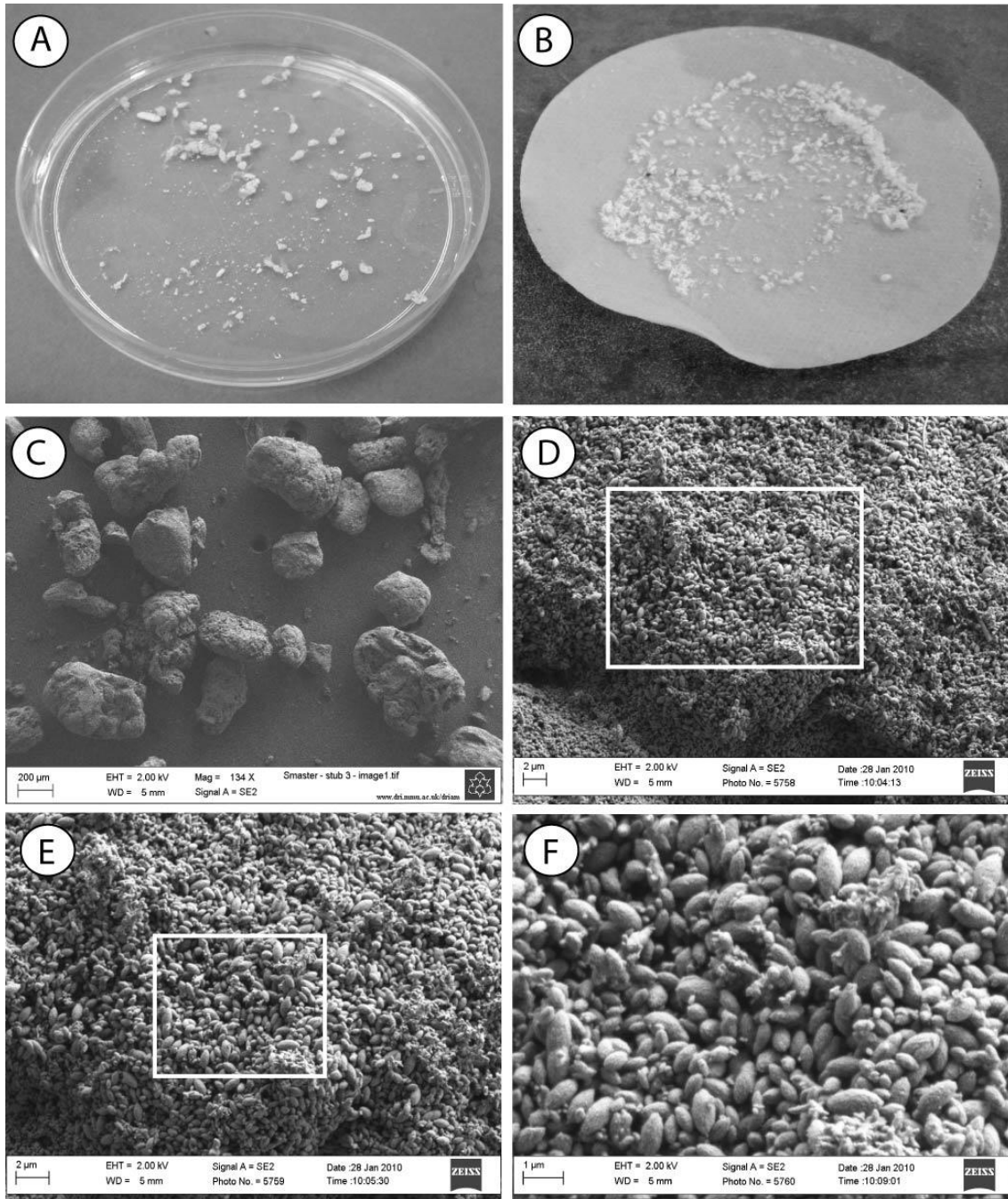
Supplementary Figure 2. Carbonate samples produced by Schoolmaster (*Lutjanus apodus*). (A) Mucus pellets excreted by Schoolmaster prior to cleaning (petri-dish is ~70 mm diam.). (B) Crystallite agregates on filter papers after 'cleaning' with dilute bleach (filter paper is 46 mm diam.). (C) SEM image of individual carbonate pellets that are retained after cleaning on the filter papers. (D, E) Detail of pellet surfaces showing the dense packing of large numbers of individual crystallites. (F) Close-up of area in (E) showing detail of individual ellipsoidal crystallites.
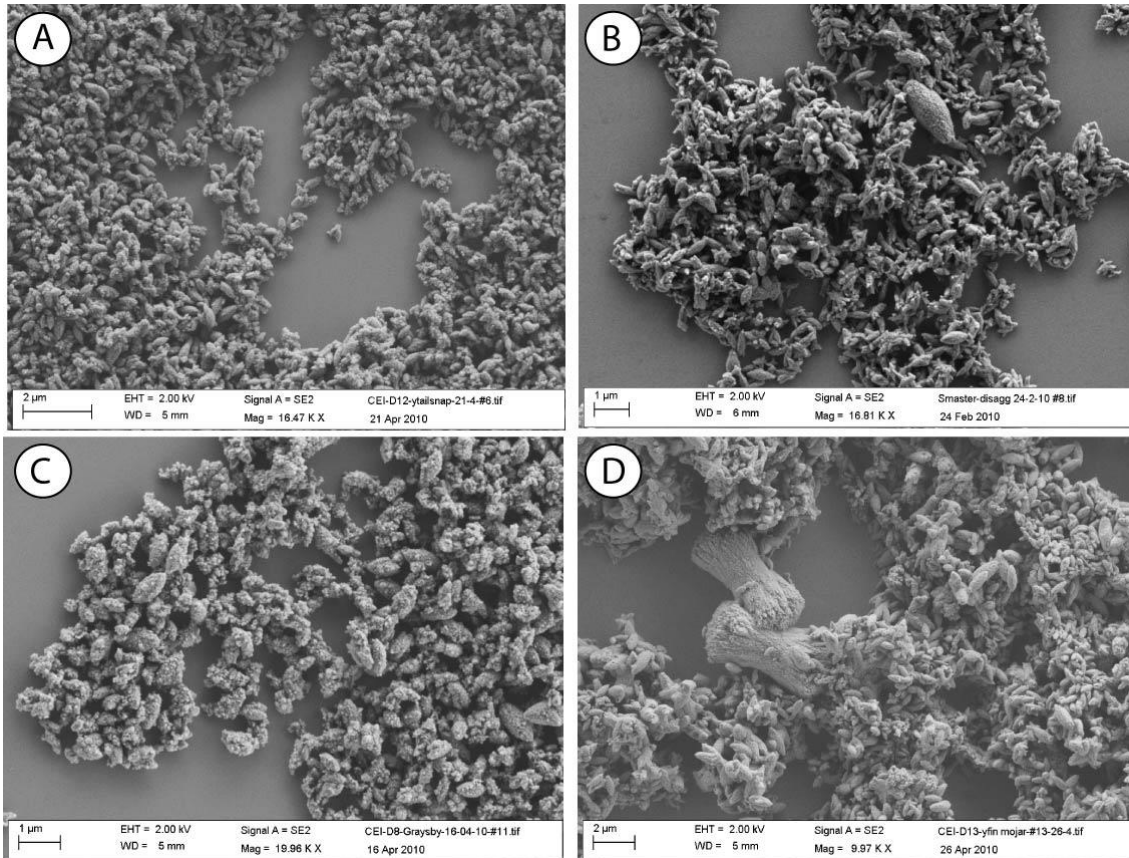
Supplementary Figure 3. Samples from various fish species following disaggregation in an ultrasonic bath: (A) Yellowtail snapper (*Ocyurus chrysurus*), (B) Schoolmaster (*Lutjanus apodus*), (C) Graysby (*Cephalopholis cruentatus*), and (D) Yellowfin mojarra (*Gerrus cinereus*). Samples were pipetted onto silica plates and oven-dried (400oC) prior to SEM analysis. In all cases disaggregation is seen to release individual crystallites and clusters of crystallites that are morphologically identical to those described for the individual species (see Supplementary Figures. 4-14), along with varying amounts of fine-grained amorphous carbonate precipitates.

Supplementary Figure 4 - Silver Jenny (*Eucinostomus gula*)
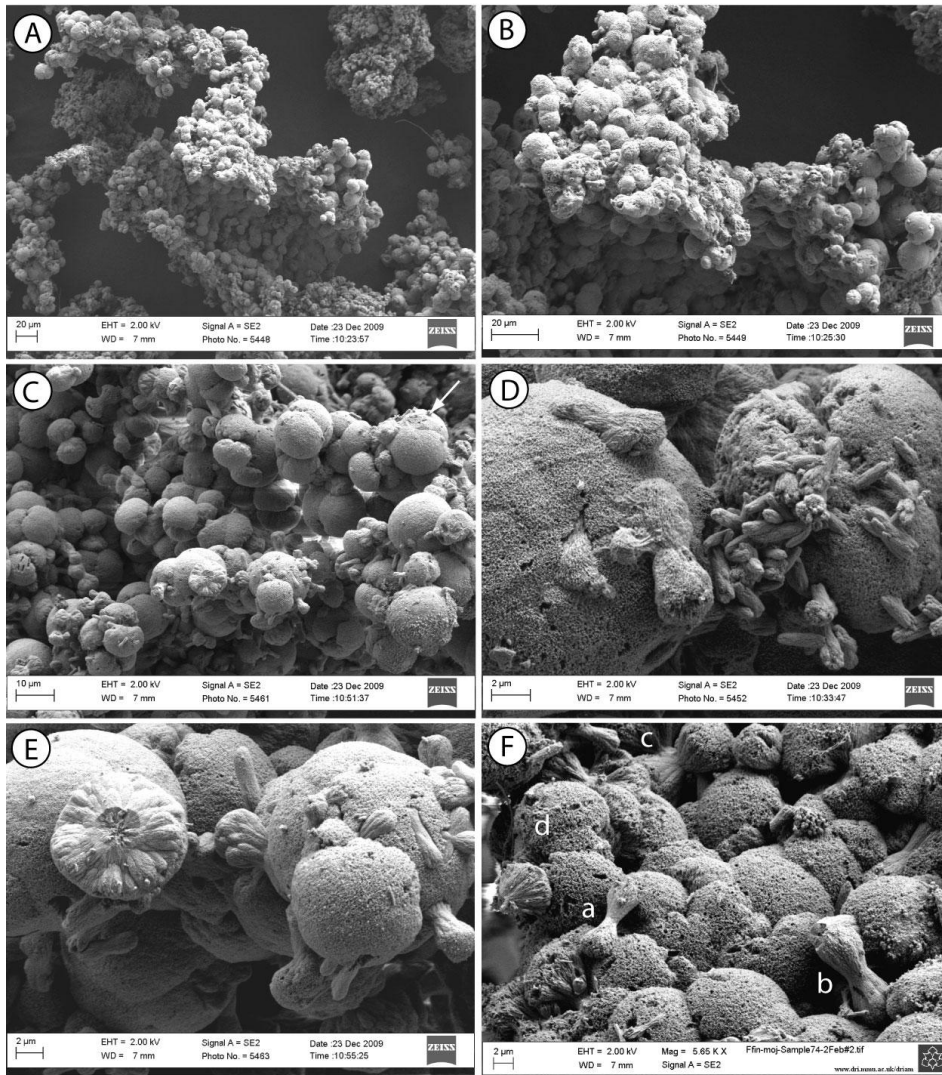
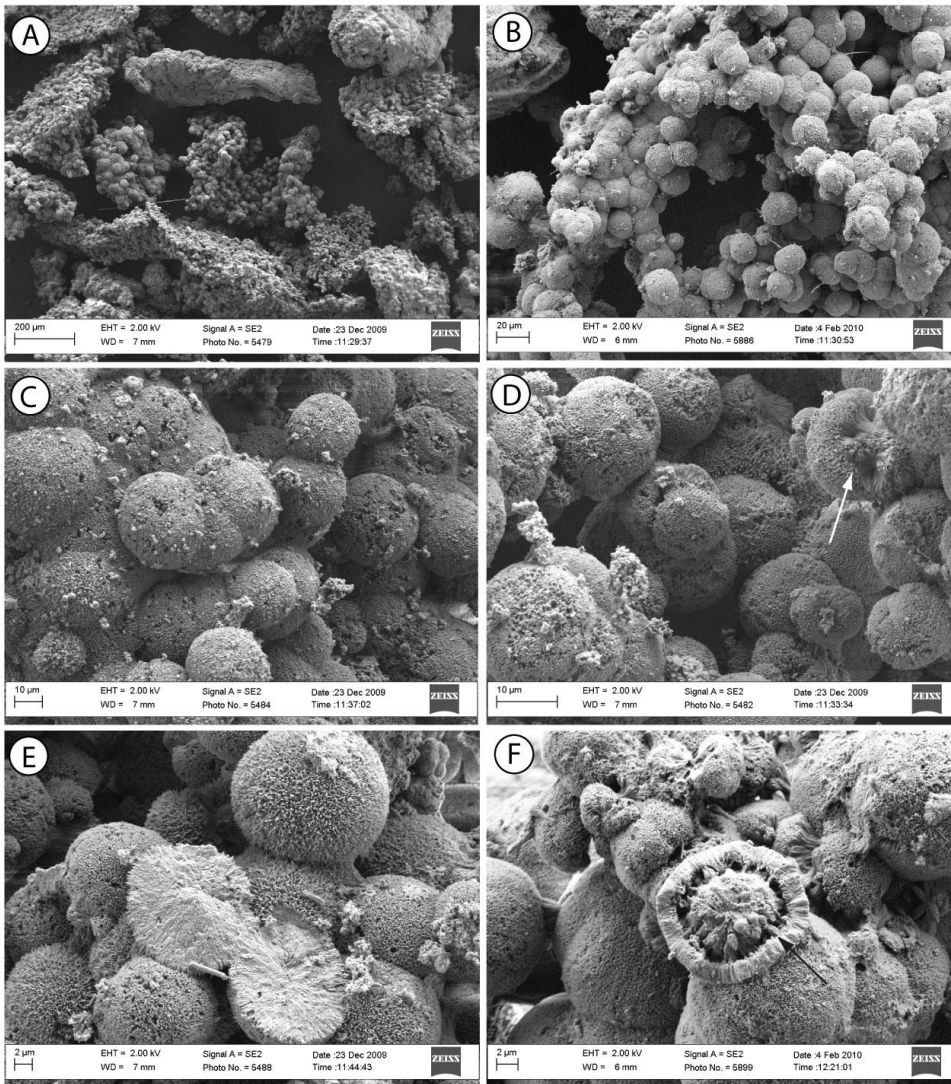**Carbonate pellets and crystallite morphologies:** Silver Jenny produce highly irregular shaped pellets up to ~1.5 mm in length (Image A). These have a relatively open crystallite packing structure and comprise dominantly spheroidal crystallites (Image B). Individual crystallites typically range in size from ~5-15 mm in diameter (Image C), and occur both as discrete spheres and, occasionally, as multi-lobed aggregations of spheres where some degree of intergrowth between adjacent spherical crystallites appears to have occurred (Image C - arrowed). There is some evidence for variation in modal grain diameters between pellets. In some instances a range of secondary crystallite structures are developed on the surfaces of spheres, these comprising elongate and semi-dumbbell shaped crystals (Images D and E). These are similar to those observed in some other fish species. In some cases these surficial crystallites are partially enclosed within the external surfaces of the larger spheres (Images D and E). Rare fragmented examples provide some indication of the internal crystallite structure of the spheres which appear to have developed via the growth of discrete fibrous bundles radiating out from a central nucleus (Image E). Evidence of the pre-spheroidal phases of crystallite growth can be seen in some samples where a sequence from small dumbbell-shaped forms (Image F - stage a), through progressively more bulbous dumbbell forms (Image F - stages b and c) to late growth stage spheres (Image F - stage d) occur.

Crystallite composition: EDX analysis indicates that the dominant spheroidal forms observed in Silver Jenny are high Mg-calcite crystals (average 18.6 +/- 2.7 mole % $MgCO_3$ (range 14.7 - 25.6); n = 50 analyses).

Typical EDX spectra from spherical crystal forms produced by Silver Jenny
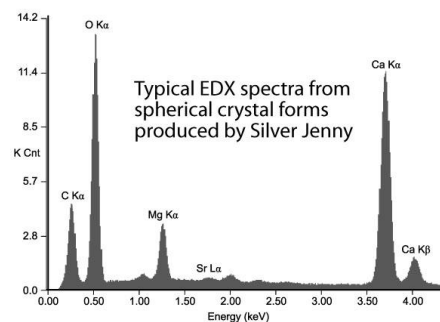
## Supplementary Figure 5 - Bonefish (*Albula vulpes*)

Carbonate pellets and crystallite morphologies: Bonefish produce irregularly shaped carbonate pellets up to ~ 3 mm in length (Image A), within which crystallite packing is relatively open (Image B). The crystallites themselves exhibit a strongly spheroidal morphology and are typically in the size range of ~10 to 30 mm in diameter (Image B), although occasional crystallite forms to ~ 40 mm diameter occur. In most cases crystallites appear as semi-discrete spheres, but it is typically the case that adjacent spheres are partially intergrown and, in some cases, exhibit a clear multi-lobate morphology (Image C). There is some evidence for variation in modal grain diameters between pellets. Crystal fibre terminations are commonly exhibited on the surfaces of spheres (Image E), although it appears that in some cases these may be a surfical crystallite overgrowth. The nature of the earliest spherical growth forms is slightly unclear, but in some cases bulbous dumbbell morphologies are observed (Image D - arrowed) which appear to be a precursor stage of complete spheroidal crystal development. This proposed mode of crystallite evolution is supported in rare fractured examples (Image E) where dense, radial growth of crystal fibers is evident. However, rare broken examples of spheres also occur which exhibit a very different internal structure (Image F) and in these cases a discrete phase of external radial crystal growth appears to have occurred around a central crystalline nucleus that has a more aggregated pelloidal fabric. These pelloidal structures are ~0.5-1 mm in diameter. Some degree of connection between these two stages is evident (Image F - arrowed).

Crystallite composition: EDX analysis indicates that the dominant spheroidal crystalline forms produced by Bonefish are high Mg-calcite crystals (average 23.1 +/- 5.5 mole % $MgCO_3$ (range 15.9 - 31.4); n = 50 analyses). Note that many spectra show a small, but discernible phosphorus peak.

Typical EDX spectra from spherical crystal forms produced by Bonefish
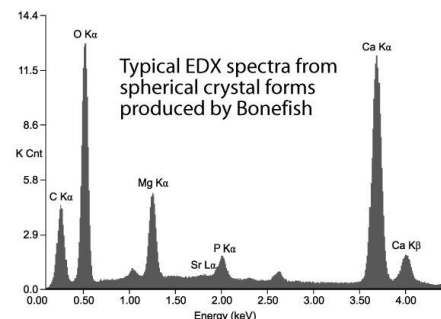
## Supplementary Figure 6 - Barracuda (Sphyraena barracuda)
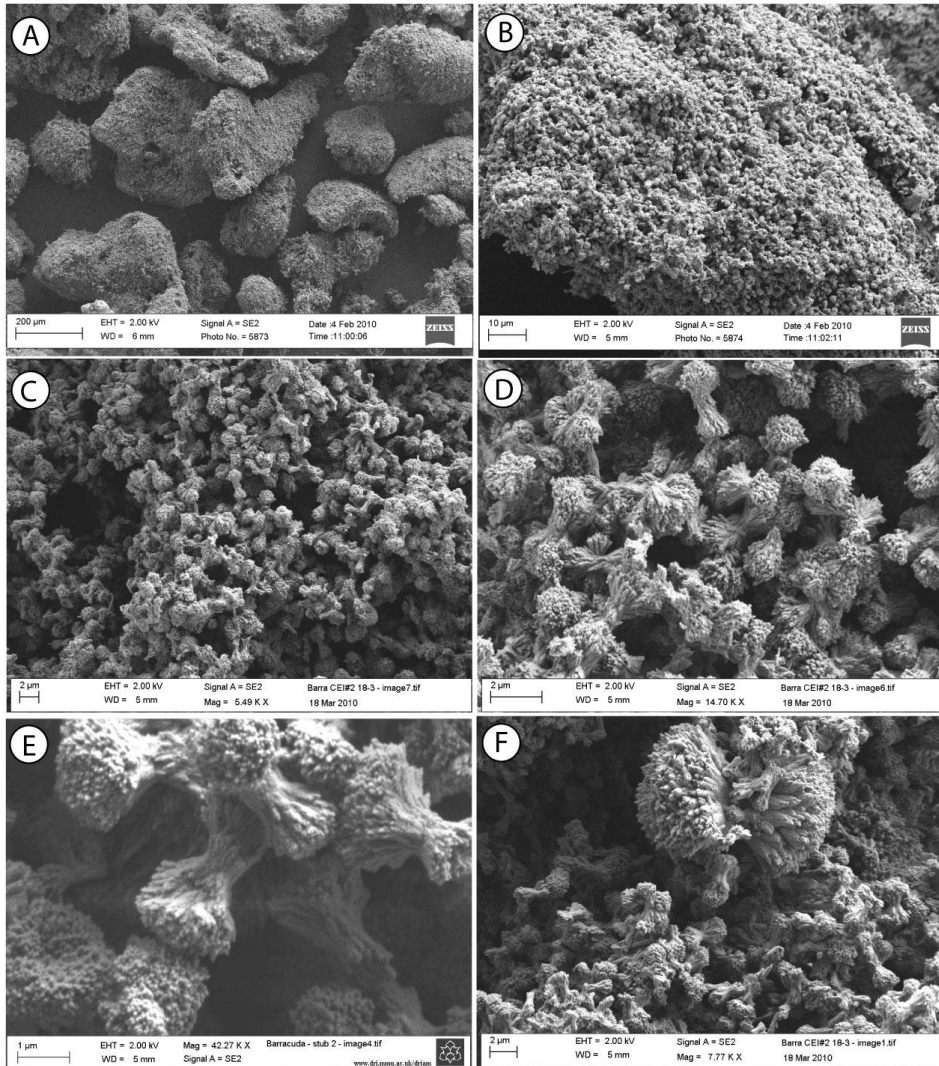
Carbonate pellets and crystallite morphologies: Barracuda produce irregular, rough surfaced carbonate pellets typically up to ~2-2.5 mm long (Image A). These are characterised by densely packed crystallites (Image B), but which nonetheless retain a quite open inter-crystalline packing arrangement (Images B and C). Pellets comprise very large numbers of individual crystallites (Image C) and these exhibit a distinctive dumbbell morphology (Image D). These crystallite forms are typically ~1.5 to 2 mm long (Image E) and appear very uniform in most pellets in terms of size and shape. In a few few cases apparent precursor crystallite forms are observed - these comprising more elongate 'wheat-bundle' type morphologies. Individual dumbbells exhibit a highly fibrous crystalline texture (Image E) with individual fibres radiating from a central (medial) nucleation point. Interestingly, in a very few pellets crystallites of markedly different sizes occur. Image F shows a background matrix of the typically small-sized dumbbells (~1.5 to 2 mm long) but within which much larger dumbbell forms occur - these are in the range ~10 to 15 mm long. These have relatively more bulbous terminal points than the smaller crystalline forms, but again, exhibit a clear fibrous crystalline structure. No intermediate crystal sizes were observed.

Crystal composition: EDX analysis indicates that the Barracuda produce high Mg-calcite crystals (average 37.1 +/- 5.4 mole % $MgCO_3$ (range 28.1 - 48.9); n = 50 analyses).

Typical EDX spectra from dumbbell crystallite forms produced by Barracuda
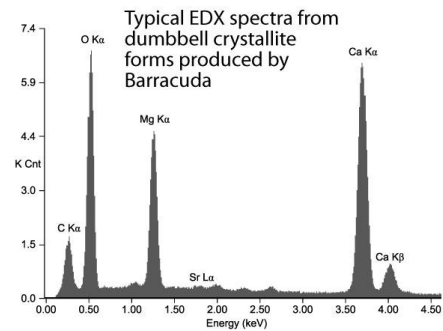
## Supplementary Figure 7- Grunt (Haemulon sp.)
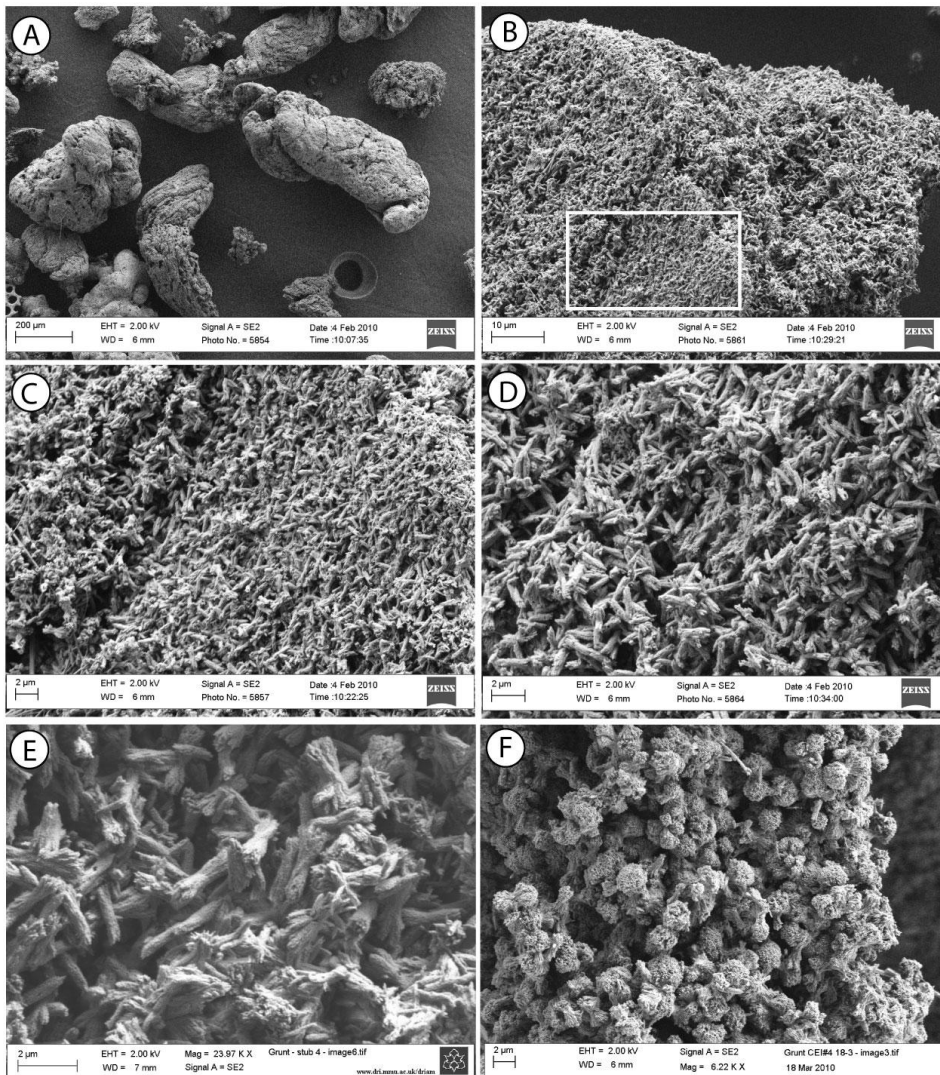
Carbonate pellets and crystallite morphologies: Grunts produce elongate and convoluted carbonate pellets that are typically up to ~ 1 mm in length and 0.5 mm in width (Image A). These pellets are densely packed with crystallites (Images B and C) but have a relatively open inter-crystalline packing arrangement (Image D). Individual crystallites exhibit a very distinctive straw-bundle morphology with individual crystallites being quite ragged in appearance, especially at their terminal points (Image E). Crystallites are relatively uniform in size, typically being ~1-2 mm long and ~ 0.25-0.5 mm wide. Less clearly developed (narrower and shorter) crystallites occur in some samples and represent possible precursor forms. In addition, some samples contain crystallites with a more ellipsoidal morphology that may also represent early stages of crystallites growth. In a very few cases crystallites with a distinct 'maltese cross' morphology occur within the mass of straw bundle forms. In addition, in some pellets crystallites with a distinctive dumbbell morphology occur (Image F). These appear to be morphogenetically related to the straw-bundle forms, having developed through crystallite enlargement along their terminal ends.

Crystal composition: EDX analysis indicates that the straw-bundle crystallite forms produced by Grunt are high Mg-calcites (average 29.0 +/- 5.3 mole % $MgCO_3$ (range 19.4 - 34.6); n = 50 analyses).
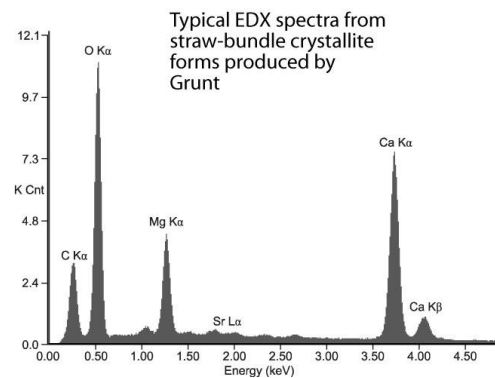
Supplementary Figure 8 - Schoolmaster (Lutjanus apodus)
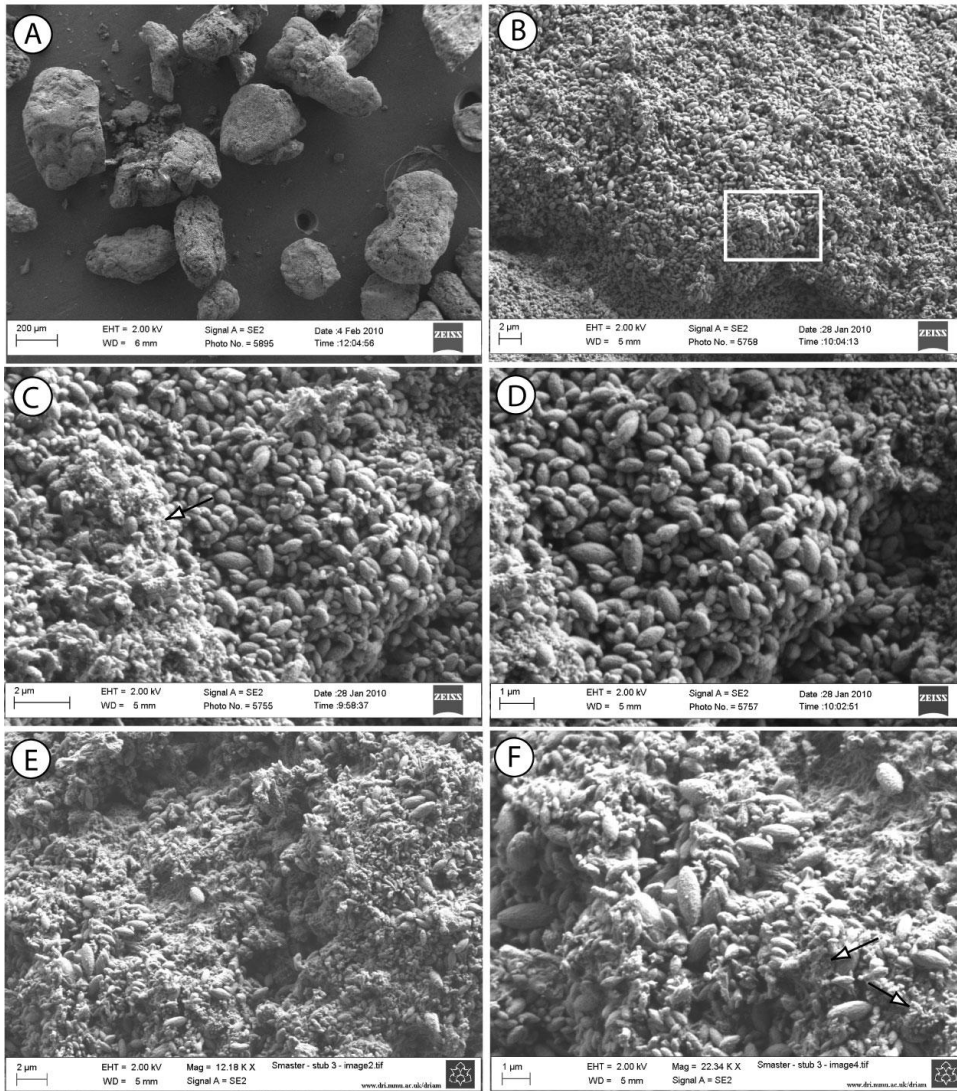
Carbonate pellets and crystallite morphologies: Schoolmaster produce sub-angular to sub-rounded shaped carbonate pellets that are typically up to 1-2 mm in size (Image A). These are very densely packed (Image B) and pellets contain very large number of individual crystallites (Image C). Crystallites exhibit a very distinctive ellipsoidal morphology (Image D) and are typically in the size range 0.5-1 mm long and ~ 0.25-0.5 mm wide (although crystallites up to ~2 mm in length do occur). However, most pellets contain ellipsoidal crystallites of varying size (Images E and F) implying that the large ellipsoids have developed from smaller crystallites of the same morphology. In addition, it is common to observe the presence of more amorphous fine-grained carbonates between the large crystallite forms (Images C and F - arrowed) - these may represent precursor (very early) phases of carbonate precipitation.

Crystallite composition: EDX analysis indicates that the dominant ellipsoidal crystallite forms produced by Schoolmaster are high Mg-calcites (average 37.2% +/- 7.1 mole $MgCO_3$ (range 23.9 - 50.5); n = 50 analyses).

Typical EDX spectra from ellipsoidal crystals produced by Schoolmaster
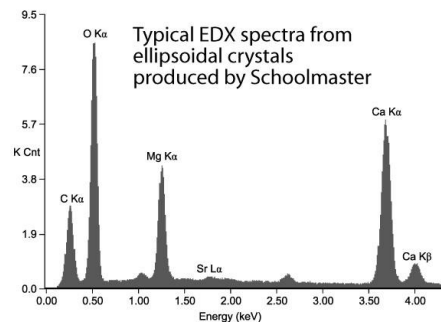
Supplementary Figure 9 - Flounder (Bothus lunatus)
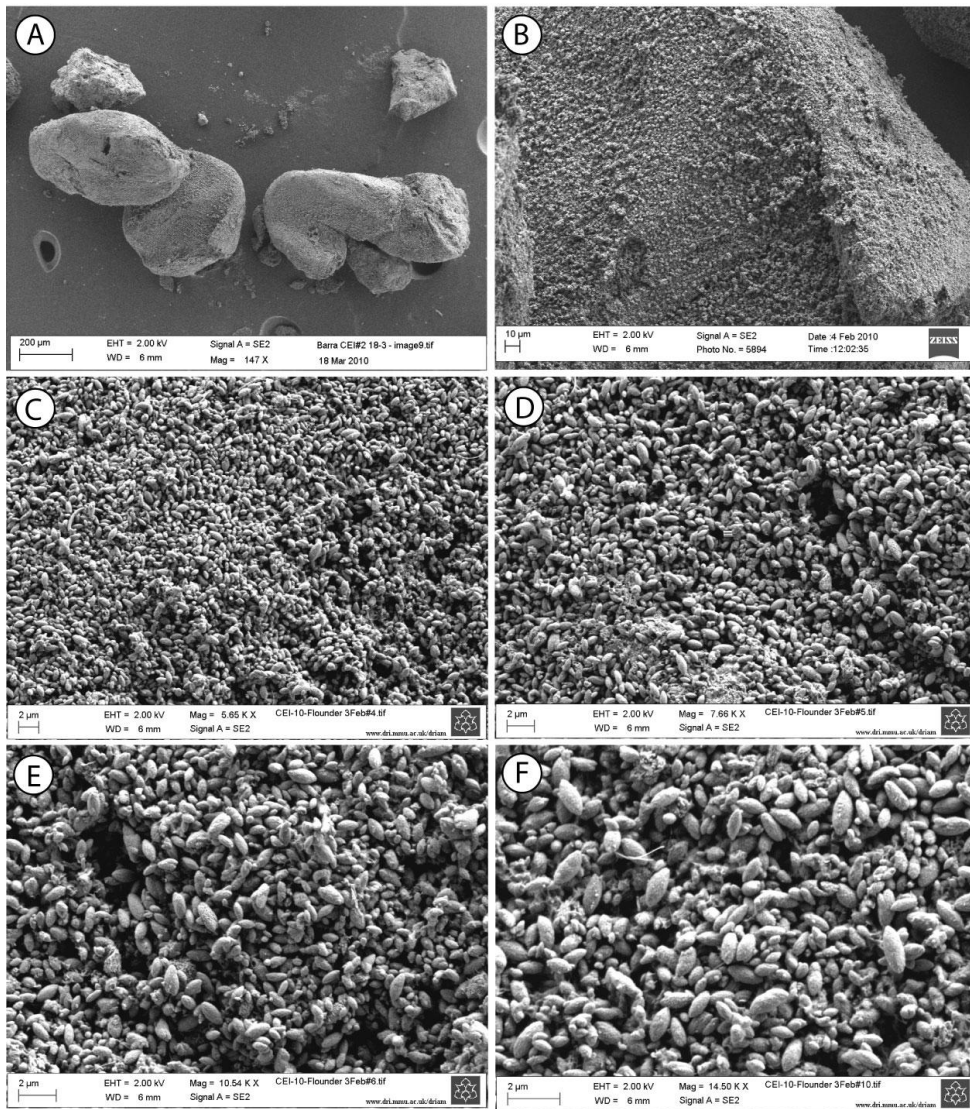
Carbonate pellets and crystallite morphologies: Flounder produce sub-rounded to elongate carbonate pellets that are typically up to 1 mm in size (Image A). These are very densely packed (Image B) and pellets contain very large number of individual crystallites (Image C). Crystallites exhibit a very distinctive ellipsoidal morphology (Image D) and are typically in the size range 0.5-1 mm long and ~ 0.25-0.5 mm wide (although crystallites up to ~1.75-2 mm in length do occur). No other obvious precursor or later crystalline growth stage morphologies are observed. However, most pellets contain ellipsoidal crystallites of varying size (Images E and F) implying that the large ellipsoids have developed from smaller crystallites of the same morphology.

Crystal composition: EDX analysis indicates that the ellipsoidal crystallites fromed by Flounder are high Mg-calcites (average 36.4 +/- 4.6 mole % $MgCO_3$ (range 26.3 - 44.9); n = 50 analyses).

Typical EDX spectra from ellipsoidal crystals produced by Flounder
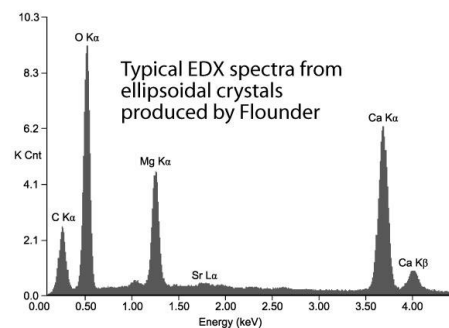
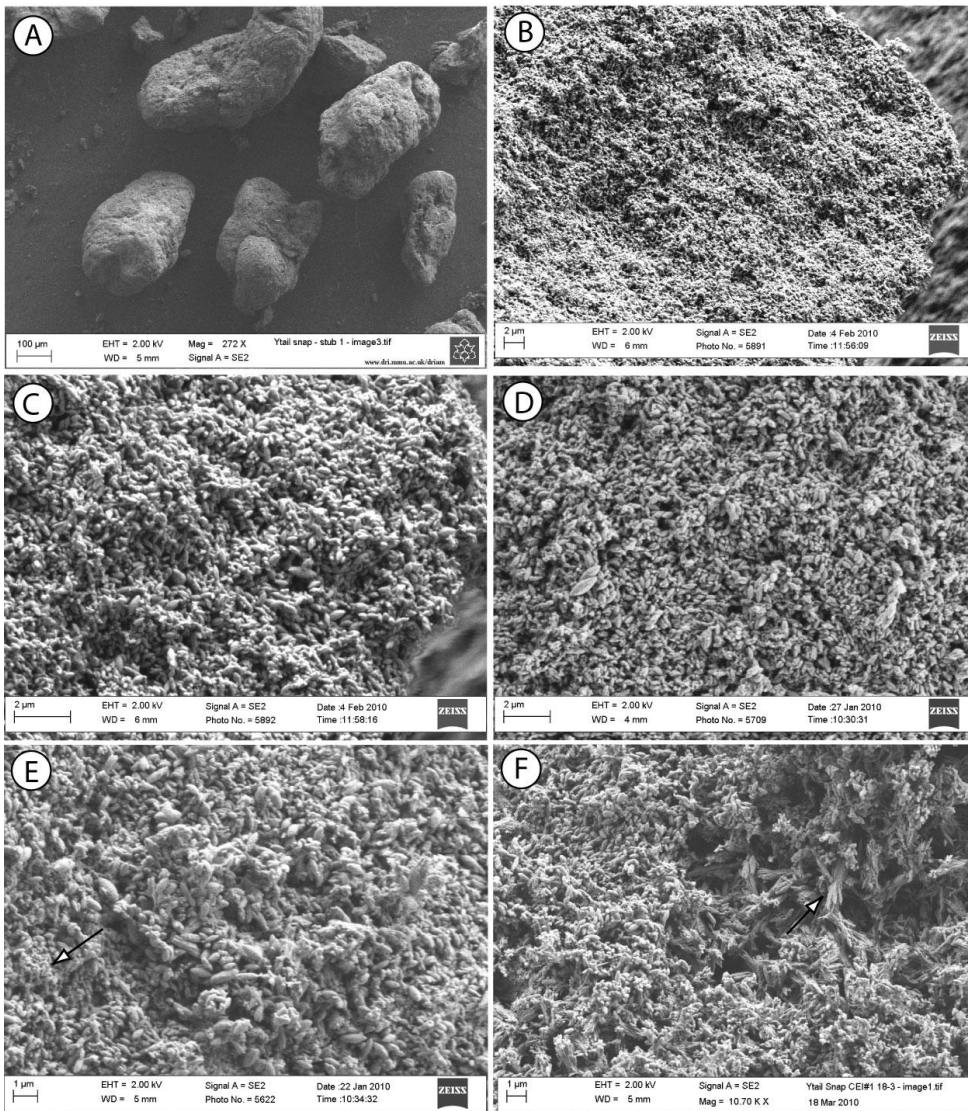## Supplementary Figure 10 - Yellowtail snapper (Ocyurus chrysurus)

Carbonate pellets and crystallite morphologies: Yellowtail snapper produce sub-rounded to elongate shaped carbonate pellets that are typically up to ~2.5 mm in size (Image A). Pellets are very densely packed (Image B) and contain very large numbers of individual crystallites (Image C). Crystallites exhibit a very distinctive ellipsoidal morphology (Image D) and are typically <1 mm long and < 0.25 mm wide (although crystallites up to ~1.5 mm in length do occur). In some samples more amorphous fine-grained carbonates occur between the large crystallite forms (Image E - arrowed) - these may represent precursor (very early) phases of carbonate precipitation. In addition, in a few samples crystallites with a more 'straw bundle' type morphology occur (Image F - arrowed) and these may represent slightly later stages of crystallite development i.e., they may have evolved from the more common ellipsoidal forms.

Crystallite composition: EDX analysis indicates that the Yellowtail snapper produce high Mg-calcite crystals (average 34.5 +/- 3.4 mole % MgCO3 (range 28.5 - 40.2); n = 50 analyses).

Typical EDX spectra from ellipsoidal crystals produced by Yellowtail snapper
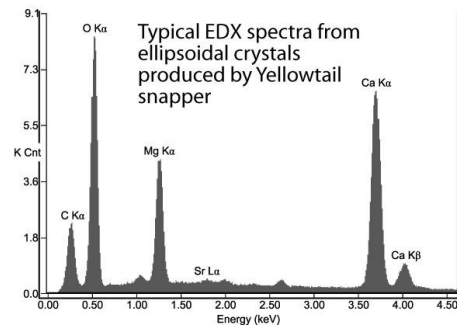
Supplementary Figure 11 - Yellowfin mojarra (*Gerrus cinereus*)
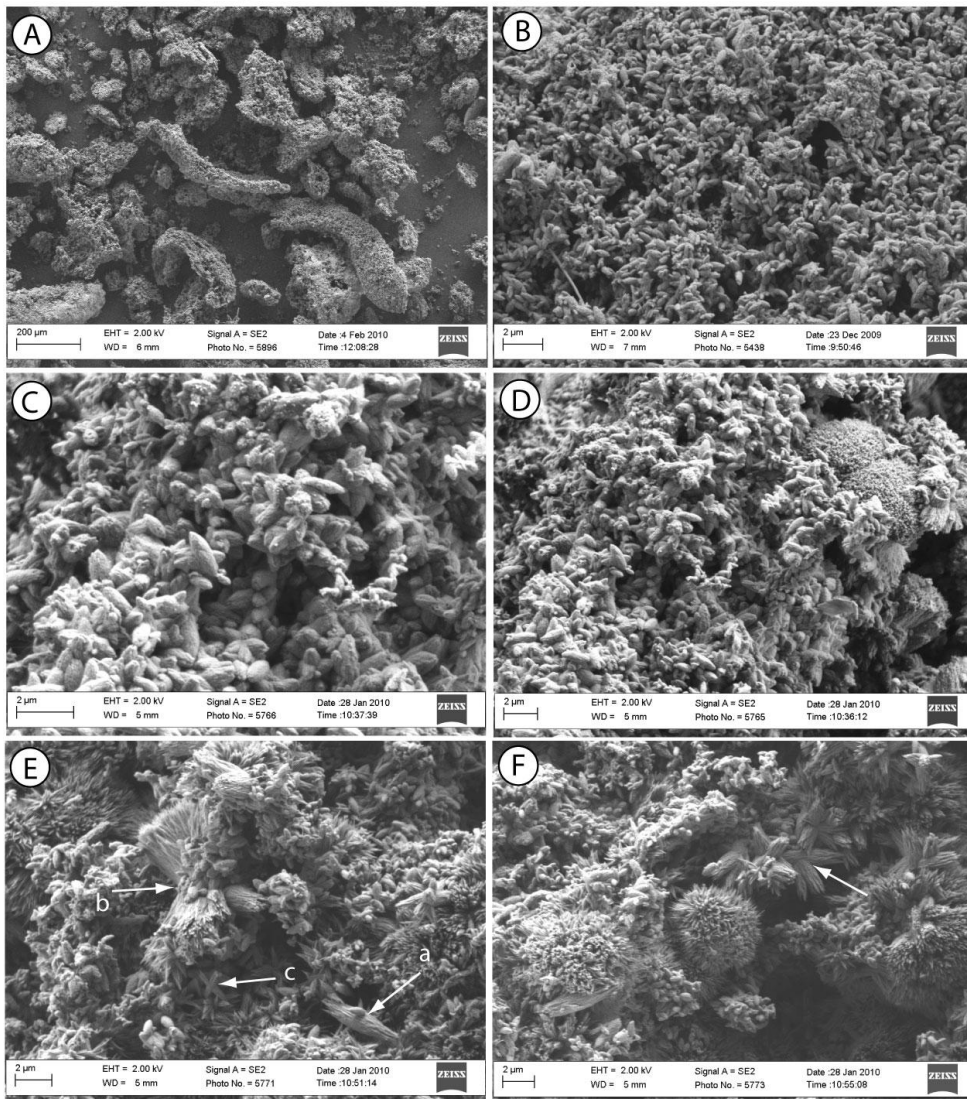
Carbonate pellets and crystallite morphologies: Yellowfin mojarra produce highly irregular shaped pellets, some elongate and up to ~1 mm long, others sub-angular to sub-rounded and up to ~0.5 mm diameter (Image A). The pellets comprise large numbers of typically small (averaging ~1 mm long) ellipsoidal crystallites (Image B). Crystallites are not densely packed within pellets and disaggregate relatively easily. Whilst the ellipsoidal crystallite form predominates, crystallite size and form is quite variable. For example, ellipsoidal crystallites exhibit a range of sizes (from <0.5 mm to ~ 2 mm long) (Image C). In addition, a diverse range of other crystallite morphologies are observed in some pellets. Importantly, these always co-occur with, but are volumetrically subordinate to, the ellipsoidal forms (Image D). The other crystallite morphologies seen are: i) those with a splayed ellipsoidal form - where the terminal points of the crystallites taper and are highly fibrous. These are larger than the ellipsoidal forms (up to ~ 3 mm long) (Image E - arrow a); ii) crystallites with a well-developed dumbbell morphology (up to ~ 5 mm long) (Image E - arrow b); iii) crystallites with a fibrous rod-like morphology (up to ~ 3 mm long) (Image E - arrowed) - sometimes developed in a distinctive cross arrangement (Image E - arrow c), in other cases exhibiting an intergrown rod arrangement (Image F - arrow); and iv) crystallites with a distinct spheroidal form - these are typically up to ~ 10 mm diameter (Images D and F). It is possible that these are part of a morphogenetic sequence of forms.

Crystallite composition: EDX analysis indicates that the ellipsoidal crystallite forms produced by Yellowfin mojarra are high Mg-calcites (average 20.3 +/- 5.6 mole % $MgCO_3$ (range 9.2 - 26.4); n = 50 analyses).
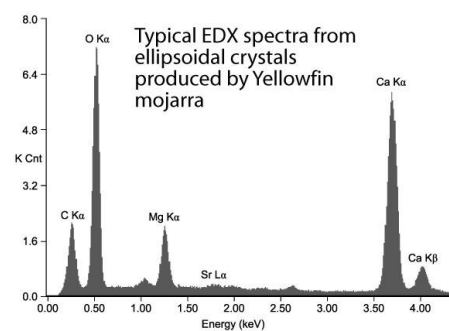
Supplementary Figure 12 - Red Hind (Epinephelus guttatus)

A — 200 μm | EHT = 2.00 kV | WD = 7 mm | Mag = 106 X | Signal A = SE2 | Red Hind - stub 5 - image1.tif | www.dri.mmu.or.uk/drism

B — 20 μm | EHT = 2.00 kV | WD = 5 mm | Signal A = SE2 | Date :4 Feb 2010 | Photo No. = 5867 | Time :10:44:22 | ZEISS

C — 2 μm | EHT = 2.00 kV | WD = 4 mm | Signal A = SE2 | Date :27 Jan 2010 | Photo No. = 5735 | Time :11:57:06 | ZEISS

D — 2 μm | EHT = 2.00 kV | WD = 4 mm | Signal A = SE2 | Date :27 Jan 2010 | Photo No. = 5739 | Time :12:05:01 | ZEISS

E — 1 μm | EHT = 2.00 kV | WD = 6 mm | Signal A = SE2 | Red Hind CEI#5 18-3 - image4 .tif | Mag = 13.40 K X | 18 Mar 2010

F — 1 μm | EHT = 2.00 kV | WD = 6 mm | Signal A = SE2 | Red Hind CEI#5 18-3 - image2 .tif | Mag = 29.53 K X | 18 Mar 2010

Carbonate pellets and crystallite morphologies: Red Hind produce sub-rounded and often tapered carbonate pellets, with smooth surfaces that are typically up to 1 mm long (Image A). These are very densely packed (Image B) and pellets contain very large number of individual crystallites (Images C and D). Individual crystallites are very small (usually < 0.5 mm long) and typically these exhibit an ellipsoidal morphology (Images E and F). However, a proportion of these fine crystallite aggregations do not display a clear morphology, appearing either rather more blocky or amorphous in form.

Crystallite composition: EDX analysis indicates that the Red Hind produce high Mg-calcites (average 39.6 +/- 8.2 mole % $MgCO_3$ (range 26.7 - 45.6); n = 50 analyses).

Typical EDX spectra from ellipsoidal crystals produced by Red Hind
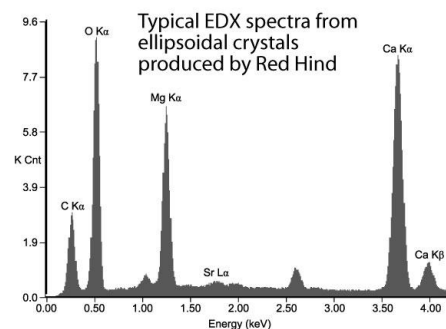
Supplementary Figure 13 - Graysby (Cephalopholis cruentatus)
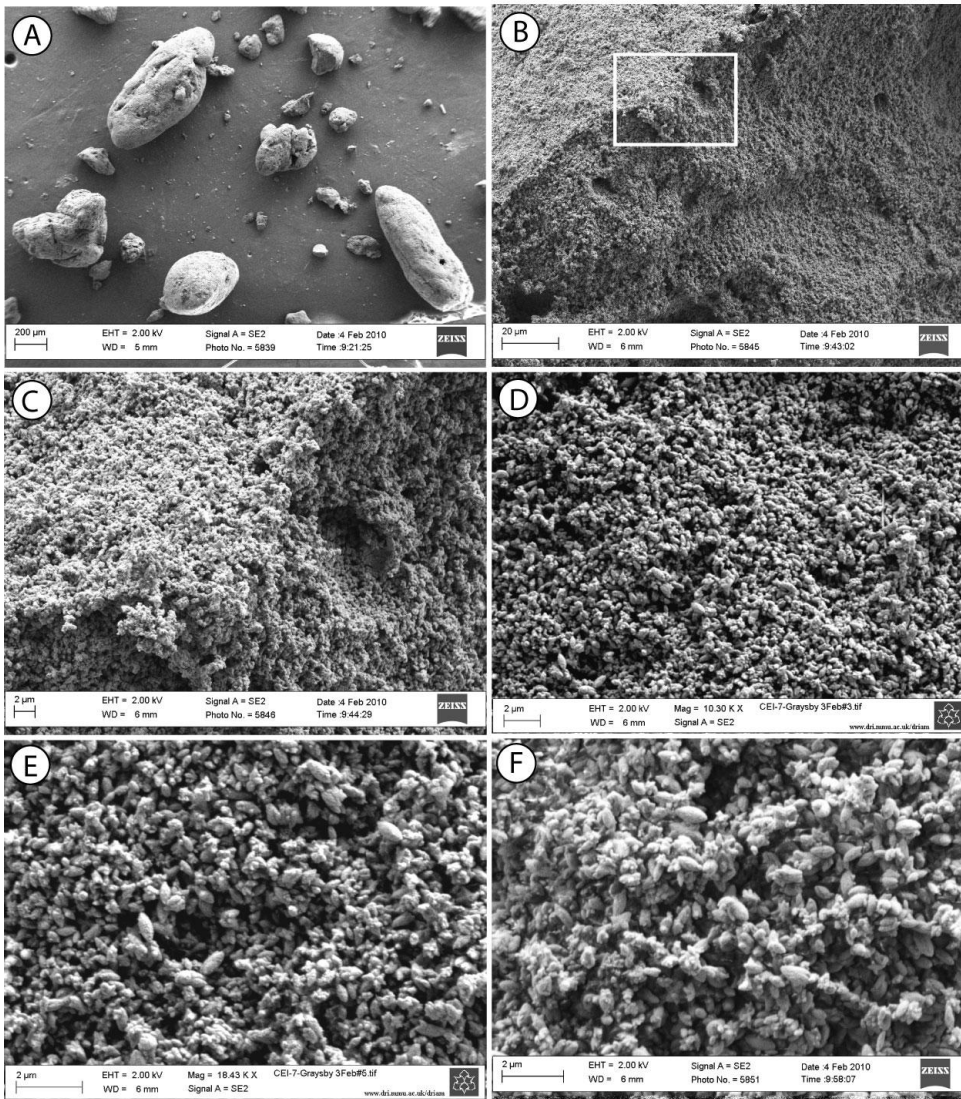
Carbonate pellets and crystallite morphologies: Graysby produce rounded, elongate, smooth surfaced pellets up to ~ 2 mm long (Image A). These are very densely packed (Image B) and pellets contain very large number of individual crystallites (Images C and D). Crystallites exhibit a very distinctive ellipsoidal morphology (Image E) and are typically in the size range 0.5-1 mm long and ~ 0.25-0.5 mm wide. However, most pellets contain ellipsoidal crystallites of varying size (Images E and F) implying that the large ellipsoids have developed from smaller crystallites of the same morphology. In addition, it is common to observe the presence of more amorphous fine-grained carbonates between the large crystallites - these may represent precursor (very early) phases of carbonate precipitation. In a very few pellets small dumbbell morphology crystallites (to ~ 2-3 mm long) have been observed.

Crystallite composition: EDX analysis indicates that the ellipsoidal crystallites produced by Graysby are high Mg-calcites (average 33.7 +/-4.7 mole % $MgCO_3$ (range 23.4 - 43.4); n = 50 analyses).

Typical EDX spectra from ellispoidal crystals produced by Graysby
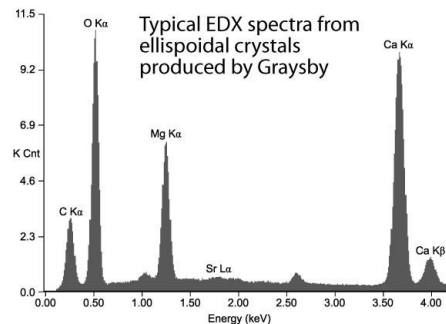
Supplementary Figure 14 - Lionfish (Pterois volitans)
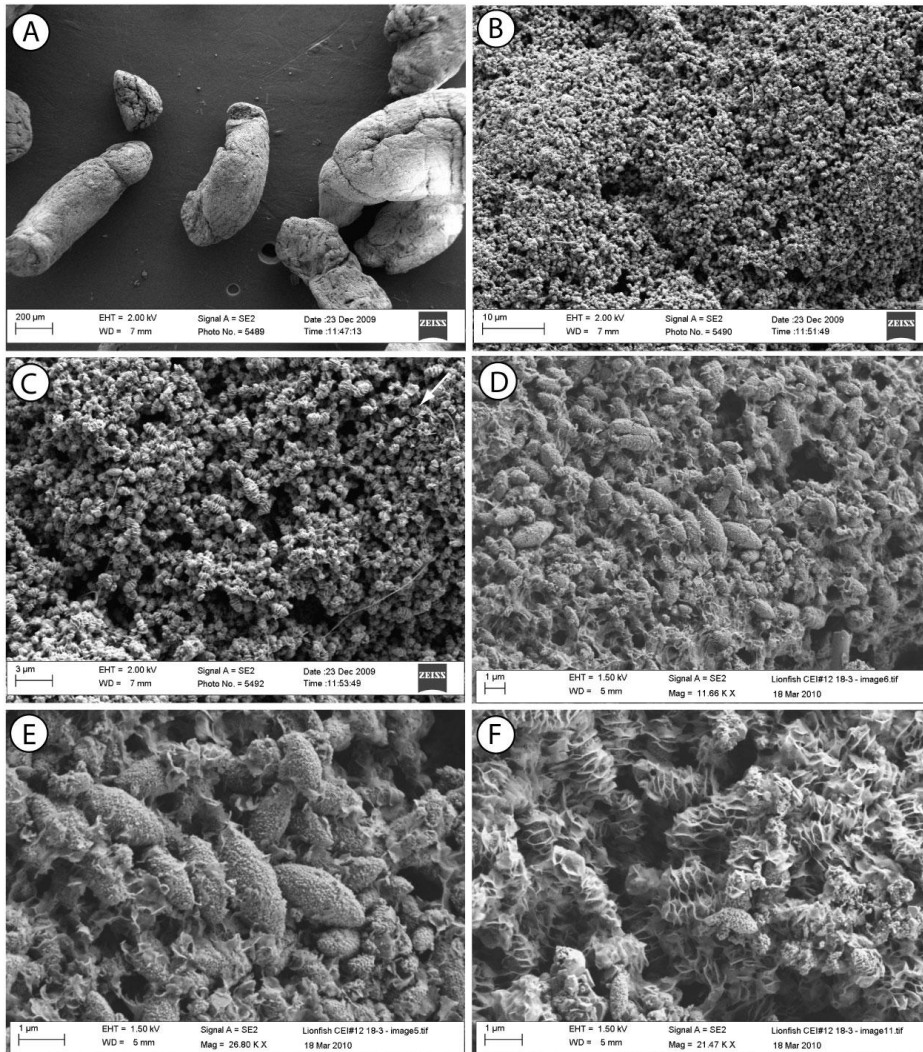
Carbonate pellets and crystallite morphologies: Lionfish produce smooth elongate carbonate pellets often with pointed terminations (Image A) that are up to ~1.5-2 mm in length. These exhibit a relatively dense crystallite packing structure (Images B and C) comprising ellipsoidal crystallites (Image D). Individual crystallites typically range in size from ~0.5 - 1.5 mm in length, but crystallites up to ~2.5mm in length also occur (Images D and E). A very distinctive feature of these crystallites is that they almost always have a fine platy, rosette type crystalline surface structure than appears as a surface coating above the primary ellipsoidal crystallite forms (Image E) and usually as a amorphous mass of fine platy, crystalline intergrowths (Image F). These coatings are intepreted as secondary precipitates. They are morpholgically identical to rosettes of dypingite (a hydroxy magnesium carbonate mineral) that has been observed forming within biofilms under highly alkaline conditions. We interpet these as products of microbially mediated carbonate mineral precipitation within the mucus coatings that surround the pellets when they are released from the fish gut.

Crystallite composition: EDX analysis indicates that the ellipsoidal crystallites produced by Lionfish are high Mg-calcites (average 34.7 +/-4.7 mole % $MgCO_3$ (range 21.6 - 43.1); n = 50 analyses).
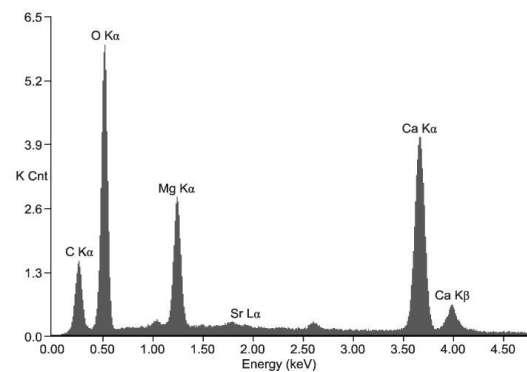
X-ray diffraction (XRD) analysis was undertaken on bulk samples collected from a sub-set of six fish species that had previously been observed to produce crystallites across the range of morphologies observed. Approximately 200 mg of each sample was crushed to a fine powder in an agate mortar, transferred to a side-loading aluminium cavity mount and analysed by X-ray diffraction in order to identify and characterise component crystalline phases. Diffraction patterns were obtained using a Siemens D-500 diffractometer equipped with a PIN diode detector, and Cu $K\alpha_{1+2}$ radiation $(\lambda = 0.154178\,\text{nm})$ generated at 40kV and 30mA. X-ray data were collected in step-scan mode from 5-65 $^{\text{o}}2\theta$ with a step increment of 0.02 $^{\text{o}}2\theta$ and a count interval of 1 s per step. Each sample was subsequently re-analysed following the addition of 20-30 mg of a silicon line standard $(a = b = c = 0.54313 \pm 2\,\text{nm})$ in order to: (1) resolve the broad, composite calcite $d_{(10.4)}$ diffraction line observed in initial diffraction patterns; and (2) use d-spacing values measured for component peaks to estimate the amount fraction of MgCO$_3$ (X_{MgCO_3}) substituted into the calcite lattice [39]. Diffraction data were collected in step-scan mode from 26.5-32.5 $^{\text{o}}2\theta$ using a step increment of 0.01 $^{\text{o}}2\theta$ and a count interval of 6 s per step. The resultant composite $d_{(10.4)}$ diffraction peak (Figs. S15a, b) were decomposed by fitting computer-generated line profiles using a non-linear, least squares pseudo-Voigt function. The number of component diffraction lines and the initial position of each line used in the decomposition procedure was selected on the basis of a visual inspection of the diffraction pattern, but the final line positions and peak profiles (peak widths) were allowed to vary until a best-fit to the original data were obtained by the peak-fitting algorithm. Resultant line positions computed for each peak were subsequently adjusted for goniometer misalignment and specimen-dependent errors using a correction based on the line position ($d_{(100)}$) measured for the silicon internal standard.

Because Mg^{2+} is the main cation that substitutes for Ca^{2+} in biogenic marine calcite [40] it is possible to use the systematic change in unit cell dimensions associated with the substitution of the smaller Mg^{2+} cation to estimate the X_{MgCO_3} of magnesian calcite with the *proviso* that ideal lattice structures may be modified by: (1) the substitution of other cations (Na$^+$, Sr^{2+}) and anions (SO$_4^{2-}$) with differing ionic radii, and water molecules [40-42]; (2) non-ideal site mixing [40,41]; and (3) lattice distortion associated with random substitution of Mg^{2+} and the rotation of CO$_3^{2-}$ [41]. Despite the availability of several published calibrations (e.g. [43]) none of these are particularly well constrained. A working curve for the relationship between $d_{(10.4)}$ and X_{MgCO_3} was, therefore, computed by fitting a linear least squares function to values of $d_{(10.4)}$ (computed from unit cell parameter data) and X_{MgCO_3} obtained from the measurement of synthetic magnesian calcites

$(0 \leq X_{MgCO_3} \leq 0.5)$ reported [41,44]. Although individual data sets are fitted most precisely by quadratic functions (see [41,44]), regression analysis of the combined data suggests that the relationship between $d_{(10.4)}$ and X_{MgCO_3} may be approximated satisfactorily using a simple linear function without any substantive reduction in the accuracy of estimates of:

$$d_{(10.4)} = -0.02873\, X_{MgCO_3} + 0.30353 \qquad (r^2 = 0.9982,\ n = 27)$$

Despite the high degree of correlation between $d_{(10.4)}$ and X_{MgCO_3} of synthetic magnesian calcites, Bischoff et al. [41] suggest that significant uncertainties in the estimate of X_{MgCO_3} $(\geq \pm 0.05\, X_{MgCO_3})$ may be anticipated for samples of biogenic origin due to the variable effects of: (1) diffraction line broadening associated with crystallite size, defect density and the relatively poor crystallinity of biosynthetic carbonates; (2) compositional heterogeneity; and (3) lattice distortion and positional disorder of substituent cations. As a consequence estimates of X_{MgCO_3} based on the decomposition of composite diffraction lines can, at best, provide only an indication of the broader chemical composition of the component calcite, and peak maxima resolved by decomposition procedures may be viewed as providing an estimate of the modal composition of one or more distinct phases.
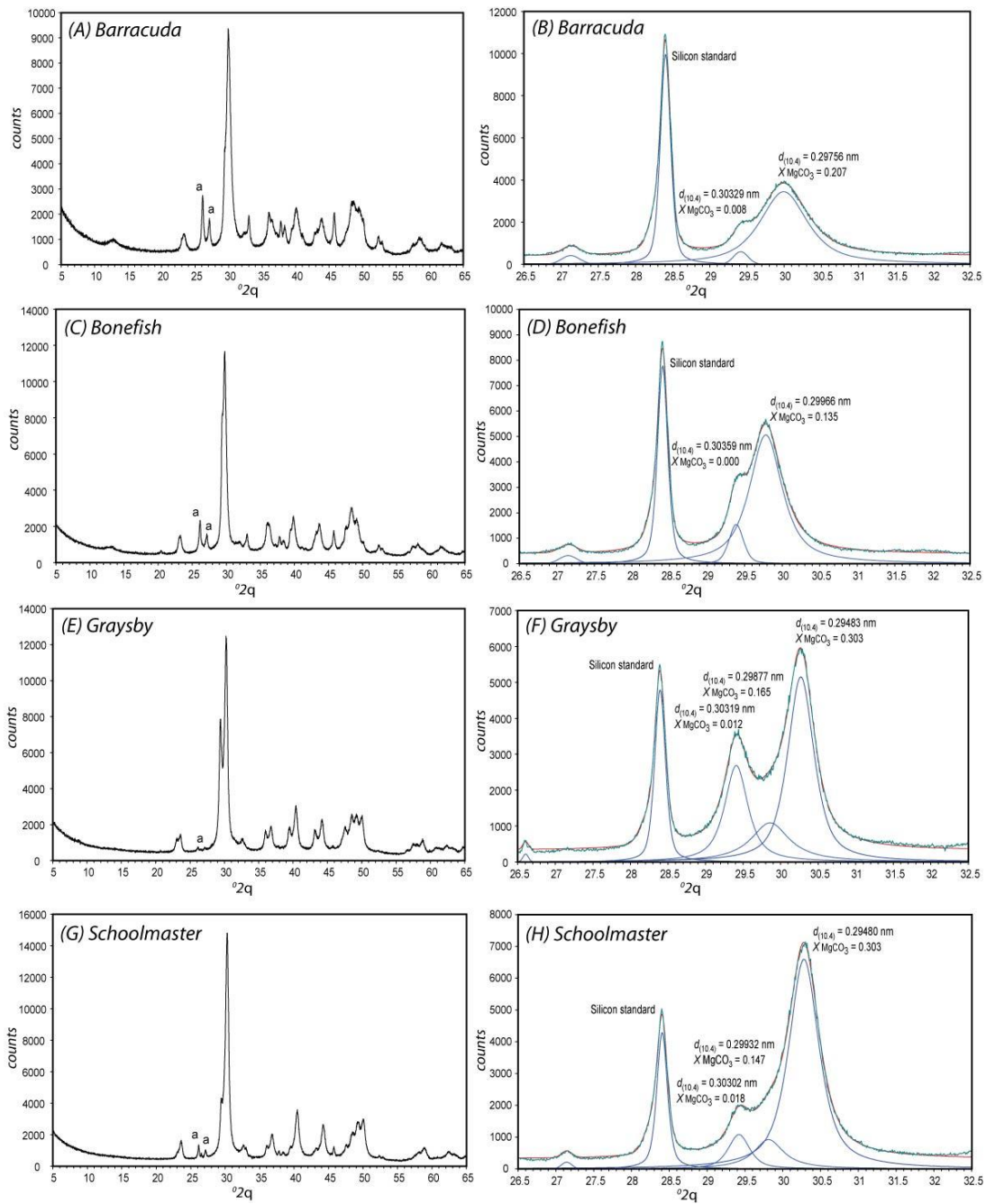
Supplementary Figure 15a. XRD traces from bulk carbonate pellet samples from (A,B) Barracuda, (C,D) Bonefish, (E,F) Graysby, and (G,H) Schoolmaster. All samples are dominated by the occurrence of calcite with varying amounts of Mg substitution. The presence of minor quantities of aragonite (a) in all samples is indicated by characteristics diffraction lines at 26.2 and 27.2 o2q.
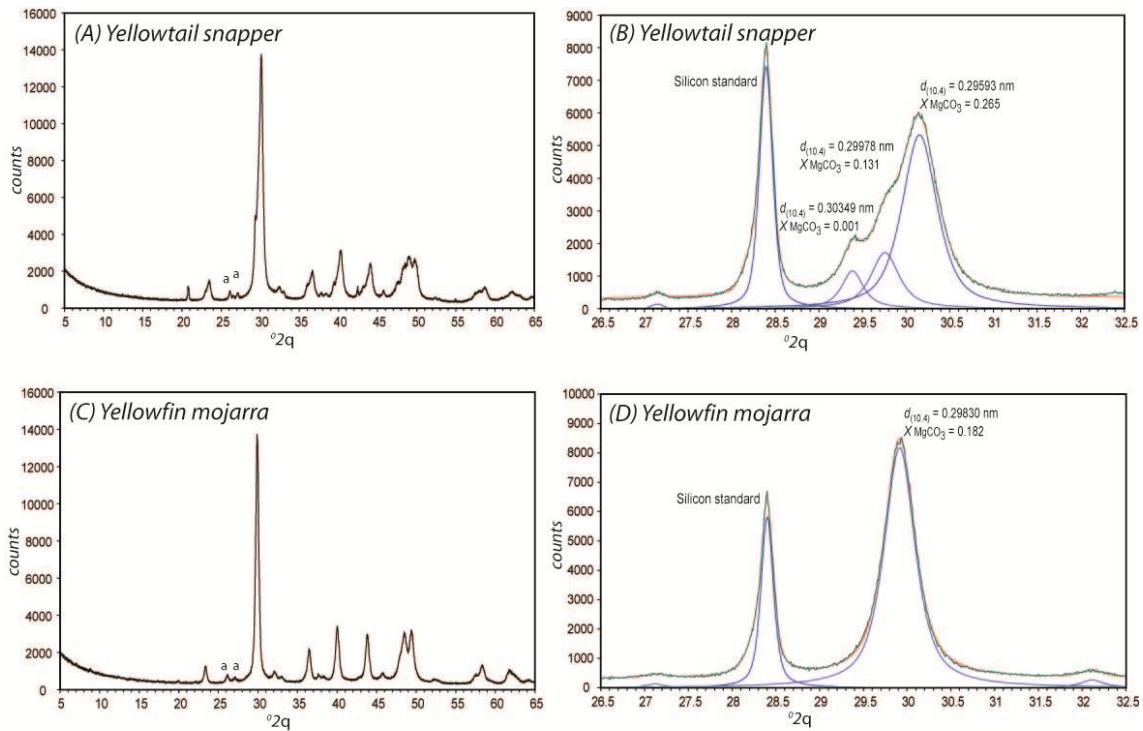
Supplementary Figure 15b. XRD traces from bulk carbonate pellet samples from (A,B) Yellowtail snapper, and (C,D) Yellowfin mojarra. Samples from Yellowtail snapper are dominated by the occurrence of calcite with varying amounts of Mg substitution. The presence of minor quantities of aragonite (a) is indicated by characteristics diffraction lines at 26.2 and 27.2 o2q. Samples from Yellowfin mojarra are also dominated by calcite with some Mg substitution. The presence of minor quantities of aragonite (a) is indicated by characteristics diffraction lines at 26.2 and 27.2 o2q.

Measurements of carbonate excretions rates by fish.

In order to determine carbonate production rates per unit of time, a sub-set of the cleaned inorganic crystal samples described above were analysed by titration using the double titration method [45] described by [21]. Briefly, crystals were ground in 20 ml of distilled water, and the resulting suspension was titrated to below pH 4.0 with 1.0 N HCl followed by immediate titration back to the starting pH with 0.1 N NaOH. During titrations samples were continuously aerated with CO_2-free air to remove all HCO_3^- and CO_3^{2-} as gaseous CO_2 during acidification, and to ensure stable pH measurement when returning to the starting pH. The differential in the number of moles of HCl and NaOH required to return to the starting pH is then equivalent to the number of bicarbonate equivalents (i.e. HCO_3^- + $2CO_3^{2-}$) in the original sample. For all titrations combination pH electrodes were used (Radiometer PHC 2401) in conjunction with handheld pH meters (either Hanna, HI 8314 or Russell, RL 200). Acid and base were added using 2 ml micrometer syringes (Gilmont Instruments, Barrington, USA) with a precision of ± 0.001 ml). The

bicarbonate equivalents content of each 24 hourly sample analysed was then converted into a molar amount of $CaCO_3$ (or $MgCO_3$) assuming that each $CaCO_3$ or $MgCO_3$ molecule yields 2 bicarbonate equivalents. The net excretion rate (μmol kg^{-1} h^{-1}) was then calculated using:

Net Carbonate Excretion Rate = Amount of $CaCO_3$ per sample / (M × t)   (1)

where M is the biomass of fish in each tank (kg), and t is the measured time interval (hours) between sample collections (recorded to the nearest minute).

Data for net carbonate excretion rate were plotted against mean body mass for each tank of a given species, in order to establish the average relationship between body mass and excretion rate for a range of Bahamas fish species (Fig. S16). The power curve fitted to the data ($y = 124.48031x^{-029452}$) describe a 2-fold increase in carbonate production for every 10-fold decrease in body mass. Note that this influence of decreasing body size on carbonate production is substantially greater than the effect on overall metabolism in fish (1.6-fold increase in metabolism for every 10-fold decrease in body size [46]). This is as predicted by Wilson et al. [19], which relates to the fact that gut carbonate production is thought to be driven by seawater drinking rates [21, 47] . In turn, drinking rate must be proportional to the osmotic water loss across the outer surfaces of the fish in order to compensate for this passive dehydration [23]. Osmotic water loss (and consequently drinking rate and $CaCO_3$ production) probably increases with smaller size more than predicted by metabolism alone for at least two reasons. Firstly, smaller animals have a larger ratio of surface area to body mass than larger animals. Secondly, the viscosity of water relative to body size becomes increasingly problematic for smaller gill-breathing animals, and so the gill ventilation (and associated osmotic water loss) needed to overcome this viscosity increases more than expected based on metabolic O_2 demand alone. Interestingly, a similarly high scaling coefficient (1.9) has been found for other osmoregulatory functions such as ion turnover in freshwater fish [48], presumably based on a similar relationship between surface area, gill ventilation and body size.
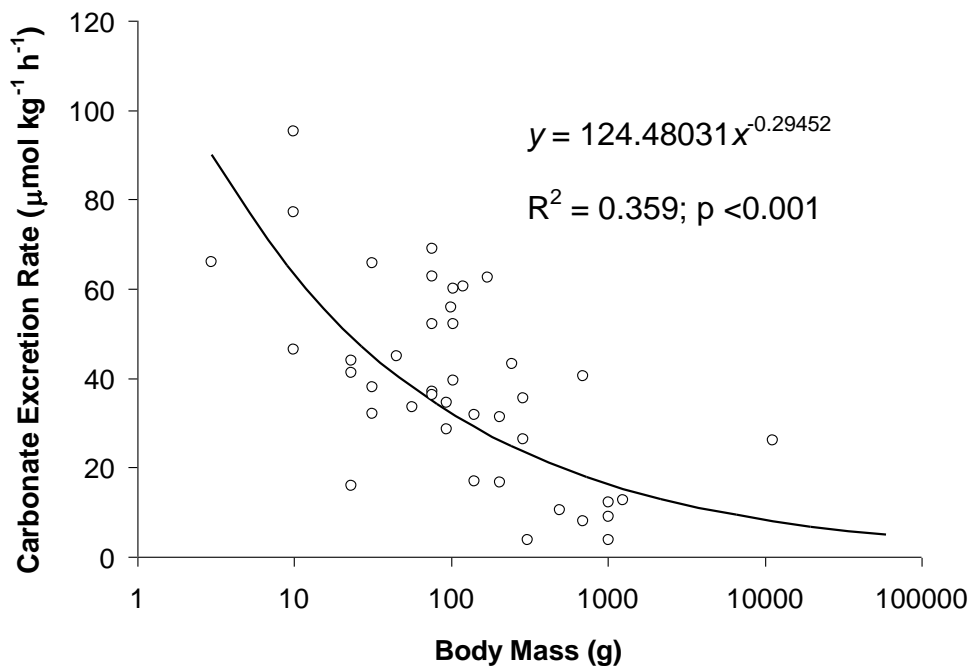
Supplementary Figure 16 The relationship between body mass (g) and the rate of carbonate excretion from the gut ($\mu mol\ kg^{-1}\ h^{-1}$) measured in a range of sizes of 11 species of teleost fish from various environments around Eleuthera, Bahamas. Collections were made at ambient temperatures (25.8±0.4 °C) and salinity (36.6±0.2). The power curve equation was generated for non-transformed body mass values (g), but body mass has been plotted on a log scale for visual clarity in this graph.

Fish biomass modeling. In order to scale measured fish carbonate production rate data to habitat scales across The Bahamas we integrated recent GIS-derived data on the areal extent of different habitat types from The Bahamas with habitat specific fish biomass data. The marine habitats, plus mangrove stands, of The Bahamas were mapped using multiple scenes of Landsat TM satellite imagery. The habitat map was created using standard classification techniques [49]. Briefly, land and deepwater was masked from each individual scene and each pixel (30 x 30 m) was assigned to a habitat type based on its spectral data. Contextual editing, which significantly increases the accuracy of tropical marine habitat maps [50], was then used to re-classify pixels to take account of generic patterns of habitat distribution (i.e., recoding some misclassified areas to the correct habitat category based on their context in the reef system). The spatial and spectral resolution of Landsat TM limits the number of habitats that can be accurately discriminated [49]. Habitats mapped within The Bahamas were (i) sand with sparse algae, (ii) mangroves, (iii) sparse seagrass, (iv) medium-density seagrass, (v) dense seagrass, (vi) gorgonian hardground, and (vii) coral-dominated reef (see [51] for more detailed habitat descriptions). The national habitat map was

created by joining the multiple classified Landsat TM scenes, and allowed the calculation of the areal extent of each habitat type.

The densities of fishes in The Bahamas were estimated using two different techniques. Visually obvious fishes were surveyed using discrete group visual fish censuses [49]. Species were divided into three groups and their density and size (to nearest centimetre) estimated along belt transects. Transect sizes and numbers were optimized using data from equivalent surveys within the Caribbean [52]. The following list of families surveyed by each diver is indicative rather than exhaustive, but transect dimensions and number were: 30 x 2 m (n = 4) for Pomacentridae, Labridae, Holocentridae, and small Serranidae; 30 x 4 m (n = 10) for Scaridae, Acanthuridae, Pomacanthidae, Chaetodontidae, Diodontidae, and Monacanthidae; 50 x 4 m (n = 5) for Haemulidae, Lutjanidae, Carangidae, Balistidae, planktivorous Labridae, large Serranidae, and other large predators. Transects for all fish groups were 30 x 2 m in mangrove habitats. Fish lengths were converted to biomass using allometric relationships [53]. Surveys of visually obvious fishes were conducted at multiple locations throughout the Bahamas archipelago (198 sites in total from Andros, Abaco, Bimini, Exumas, San Salvador, and South Caicos). Surveys at each location were stratified by habitat type (19 in total), including each of the seven habitats discriminated in the habitat map: sand with sparse algae (total of 3 surveys throughout the archipelago), mangroves (17), sparse seagrass (14), medium-density seagrass (15), dense seagrass (14), gorgonian hardground (41), and coral-dominated reef (36). The dataset is described in more detail elsewhere [36].

Visual surveys are inappropriate for censusing cryptic species, which are more accurately assessed using destructive techniques [54]. Destructive surveys of cryptic species are not available for The Bahamas. Therefore, we used a data set collected from St. Croix in the U.S. Virgin Islands (see [55]) for a more detailed description of methodologies and the dataset) as the nearest and most comparable dataset available. This study used data based on the icthyocide rotenone method to sample all fishes within blocknets ranging in size from 7.6 to 18 m^2. Fishes were surveyed at 58 sites in six habitat types, three of which were analogous to those surveyed by visual censuses in The Bahamas (patch reef, reef crest / back reef, and coral-dominated reef). Of the 228 species surveyed in the rotenone surveys in St. Croix, 83 were also recorded by visual censuses in the Bahamas. The mean total densities of these 83 species in patch reef, reef crest / back reef, and coral-dominated reef habitats in St. Croix were remarkably similar to the total densities of fishes recorded by visual censuses in The Bahamas in the same habitat types (1.9 fishes m^{-2} in St. Croix versus 1.7 in The Bahamas for patch reefs, 0.9 versus 1.0 for reef crests / back reefs, and 2.0 versus 2.1 for coral-dominated reefs). Therefore, we assumed that the data

for species recorded in St. Croix represented a suitable proxy of the cryptic fish community in The Bahamas. Densities of cryptic fishes were approximately an order of magnitude greater than densities of visually censused fishes (11.3 cryptic fishes m^{-2} versus 1.7 visually censused fishes m^{-2} for patch reefs, 14.9 versus 1.0 for reef crests / back reefs, and 10.4 versus 2.1 for coral-dominated reefs). Sizes were not available for each cryptic fish, so the mid-point between the minimum and maximum size (measured to nearest 0.1 mm) for each species at each site were used to calculate biomasses from allometric relationships [35,53]. Where species specific allometric relationships were not available, data were used from a congener or confamilial species.

Calculation of CaCO$_3$ production by habitat type. The rate of CaCO$_3$ excretion (μmol kg^{-1} h^{-1}) was calculated for each visually censused fish using the relationship between fish body mass and excretion rate established in the laboratory experiments described above (Fig. S16). Actual excretion was then calculated by multiplying the fish biomass by the rate of production, and dividing by survey area (final units = μmol carbonate, kg of fish biomass^{-1} h^{-1} m^{-2}). Carbonate production by all species was summed for each transect, and then averaged to calculate mean production per survey site. Finally, carbonate production data from the multiple sites in each habitat type were used to calculate mean production per habitat type (i.e., the mean production by fishes in that habitat type calculated from multiple sites from multiple locations within the Bahamian archipelago) (Table S2).

Habitat type	CaCO$_3$ production by visually censused fish species (μmol kg^{-1} h^{-1} m^{-2})	CaCO$_3$ production by cryptic fish species (μmol kg^{-1} h^{-1} m^{-2})	Total CaCO$_3$ production by fish (μmol kg^{-1} h^{-1} m^{-2})
Sand and sparse algae	0.001 (0.001) [3]	<0.001	0.001
Mangrove stand	1.490 (0.291) [17]	0.572	2.062
Sparse seagrass	0.013 (0.006) [14]	0.005	0.018
Medium-density seagrass	0.035 (0.014) [15]	0.013	0.048
Dense seagrass	0.053 (0.017) [14]	0.020	0.073
Gorgonian hardground	0.714 (0.116) [41]	0.274	0.988
Coral-dominated reefs	1.524 (0.189) [36]	0.751 (0.105) [7]	2.275

Supplementary Table 2 Mean estimated carbonate production by fishes in the seven habitat types mapped throughout the Bahamas archipelago. Standard errors in parentheses. Standard errors not provided for six of the habitat types because they were calculated using the estimated ratio of carbonate production between visually censused and cryptic species. Sample sizes in square brackets.

Cryptic fishes in St. Croix were not censused from six of the habitat types mapped in the Bahamas archipelago (data only from coral-dominated reefs). However, the ratio of carbonate production values by cryptic and visually obvious species in the three habitats that were surveyed

in both St. Croix and The Bahamas were reasonably consistent (0.300 on patch reefs, 0.361 on reef crests / back reefs, and 0.493 on coral-dominated reefs). Therefore, the mean of these ratios (0.384) was used to calculate the additional carbonate production by cryptic species in habitats where only visual censuses were conducted. Total carbonate production rates (Supplementary Table 3) were multiplied by the areal extent of each habitat type to estimate total production for the entire Bahamian archipelago.

Habitat type	Total habitat area (km^2)	Fish carbonate production (g/m^2/yr)	Total fish production by habitat (M kg/yr)
Sparse seagrass	14,420	0.02	0.23
Medium seagrass	27,331	0.04	1.15
Dense seagrass	11,433	0.06	0.73
Fringing mangrove	535	1.81	0.97
Gorgonian hardground	2,631	0.87	2.28
Sand (bare or with sparse algae)	54,877	0.001	0.05
Reef	350	2.0	0.70

Supplementary Table 3 Rates of carbonate production calculated from measured fish body mass and excretion rate data (see Section 4.3 above) in this study and data on total fish carbonate production by habitat type. NB. Rates are likely to be highly conservative over longer timescales as they are largely based on fish production data from outside marine reserves.

Estimates of carbonate mud production and comparisons with other mud producers. In order to compare habitat specific rates of carbonate sediment production by fish across the Great Bahama Bank (GBB) with other known sources of carbonate mud, fish carbonate production rate data (see Table S2) were first converted to a production rate in g m^{-2} yr^{-1} CaCO$_3$ (as the most widely quoted unit of sediment production) and then scaled by habitat size to quantify total carbonate production by fish for: i) each habitat type; and ii) as total for the GBB (see Table S3). Subsequently, and in order to compare calculated rates of fish carbonate production against rates reported for other known sources of tropical carbonate mud, we determined for each habitat type: i) the rates of carbonate production by other known carbonate mud producers, and ii) where relevant, the proportions reported to be subsequently converted to mud for each source (Table S4). These data were used to make a first order estimation of how much mud each source contributes to mud production within the different habitat types delineated across the GBB and against which fish carbonate production estimates could be compared. We included published data on rates of both direct inorganic carbonate precipitation (the widely discussed and controversial carbonate 'whiting' phenomena) [3,9], and data on benthic groups where mud production occurs as a result of the disaggregation and breakdown of larger skeletal grains. Most important in this context is mud-grade carbonate sourced from the breakdown of calcareous

epiphytes from seagrass blades [56-58], the disaggregation of a wide range of calcareous green algal species (*Halimeda* sp., *Penicillus* sp., *Rhipocephalus* sp. and *Udotea* sp.) [59,60], and the degradation of benthic foraminifera [12]. Where possible we used data from the Bahama Banks or, where unavailable, from Florida Bay as a geographically proximal and broadly similar depositional environment (in terms of habitat types and water depths). Exceptions are detailed in the footnotes for Table S4. We necessarily excluded any mud production sourced from the breakdown of other common skeletal sediment constituents (e.g., corals, molluscs) as there are no sufficiently reliable data available to make any assessments of the rates at which their skeletons might degrade to mud-grade carbonate.

Habitat type	Area (km²)	Seagrass epiphytes (g/m²/yr) [1]	Halimeda (g/m²/yr) [2,3]	Pencillus capitatus (g/m²/yr) [2,3]	Pencillus dumetosus (g/m²/yr) [2,3]	Rhipocephalus phoenix (g/m²/yr) [2,3]	Udotea flabellum (g/m²/yr) [2,3]	Benthic foraminifera (g/m²/yr) [5]	Whitings (g/m²/yr) [6]	Sponge bioerosion (g/m²/yr) [7]	Total mud production (g/m²/yr) [8]	Total mud production (kg/km²/yr) [8]	Total carbonate mud production by habitat (M kg/yr) [8]	Contribution of fish carbonate (%)
Sparse seagrass	14,420	40.3	18.9 (5.6)	6.4 (4.5)	6.5 (4.5)	9.1 (1.8)	1.6 (1.2)	0.6 (0.06)	7.9	0.0	66.0	66,000	951.7	0.01
Medium seagrass	27,331	90.8	3.7 (1.1)	1.3 (0.9)	1.3 (0.9)	1.8 (0.4)	0.3 (0.2)	0.6 (0.06)	7.9	0.0	102.4	102,344	2,797.2	0.04
Dense seagrass	11,433	310.2	0.0 (0.0)	0.0 (0.0)	0.0 (0.0)	0.0 (0.0)	0.0 (0.0)	0.6 (0.06)	7.9	0.0	318.2	318,220	3,638.2	0.02
Fringing mangrove	535	0.0	0.7 (0.2)	0.3 (0.2)	0.3 (0.2)	0.4 (0.1)	0.1 (0.1)	0.6 (0.06)	0.0	0.0	2.5	2578.8	1.3	70.3
Gorgonian hardground	2,631	0.0	0.7 (0.2)	0.3 (0.2)	0.3 (0.2)	0.4 (0.1)	0.1 (0.1)	0.3 (0.03)	1.9	0.0	3.5	3,508.8	14.5	24.7
Sand (bare or with sparse algae)	54,877	0.0	0.7 (0.2)	0.3 (0.2)	0.3 (0.2)	0.4 (0.1)	0.1 (0.1)	0.3 (0.03)	7.9	0.0	8.6	8,640	474.1	0.09
Reef	350	0.0	33.6 (5.04) [4]	10.1	0.0 (0.0)	0.0 (0.0)	0.0 (0.0)	0.2 (0.03)	1.9	61.1	75.1	75,100	26.3	2.63

[1] Based on data in Nelsen and Ginsburg [57] from Florida Bay ('Sparse seagrass' habitats use data from their sites with <500 blades/m²; 'Medium seagrass' habitats uses their data from sites with 501-1000 blades/m², and 'Dense seagrass' habitats uses their data from sites with >1001 blades/m². Data assumes all epiphyte production is contributed as mud grade carbonate as per previous studies [56-58].

[2] Based on data in Neumann and Land [60] from the Bight of Abaco, Bahamas. Original figures are based on a site with very high plant densities - averaging 25.7 plants/m². Our own observations from the Eleuthera Bank where green algal densities are typically <5 plants/m², and the data of Shinn et al. [2] from sites across the GBB (averaging ~1.5 plants/m²) suggest these densities are very high for the wider GBB. We thus apply their production rate data assuming plant densities of ~ 20% (equating to ~5 plants/m²). Given this, production rates are applied as 100 % in 'sparse' seagrass environments. However, because green algal abundances typically decrease with seagrass density we applied production estimates at a 50 % proportional rate (i.e., assuming 2.5 plants/m²) for 'medium' seagrass beds, and assumed no calcareous green algal production within dense seagrass beds which are typically monospecific. Low abundance is assumed within gorgonian-dominated and fringing mangrove habitats, and across bare or sparse algal covered sand habitats to which a 10 % proportional production rate (i.e., 0.5 plants/m²) figure is applied. We assume 9 crops per year for all species in our calculations after [60].

[3] Because not all carbonate produced by green algae degrades to mud-grade carbonate we apply the following mud conversion factors which are based on the algal breakdown data in [60] to each of our production estimates: Halimeda – 30%, P. capitatus – 70%, P. dumetosus – 70%, R. phoenix – 20% and U. flabellum – 70%.

[4] Based on production data in [61] for reef habitats in Antigua, whose estimates are based on sites with plant cover of 36 plants/m^2. This is high as a reefal average and we thus use a 25% proportional production rate figure (based on 9 plants/m^2) of 33.6g CaCO^3/m^2/yr. We apply the same mud conversion rate used for *Halimeda* above.

[5] Based on average production rates in [62] from Florida Bay. Data from low energy Cross Banks area are applied to all seagrass and mangrove habitats. Data from more open Buchanan Keys are applied to 'sand', 'gorgonian' and 'reef' environments. For all habitats we make an assumption that 10% of foraminiferal carbonate production is converted to mud through test breakdown (see 12 for discussion of breakdown process).

[6] Mud production from 'whitings' is based on production rates calculated by Shinn et al.[2] and is assumed representative of all environments across the GBB with the exception of protected mangrove fringed inlets where no 'whitings' assumed to occur. Rates applied at 25% for reef and gorgonian environments, reflecting lower production rates along platform margins where these habitats occur.

[7] Production of 'sponge chips' during sponge bioerosion of reef substrate. Figure based on long-term erosion rate of Rützler [63] of 70 g/m^2/yr (less 3% directly dissolved) and assumes 90% of this sediment is of mud-grade following Fütterer [64].

[8] Includes fish production data from Table S3

Supplementary Table 4 Estimated rates of sediment production by calcareous epiphytes, calcareous green algae and from the breakdown of benthic foraminifera, along with carbonate sourced from 'whitings' (inorganic carbonate precipitation). Data in parentheses are estimates of the amounts of sediment likely to be converted to mud-grade carbonate in each of the 7 delineated Bahama Bank habitats. Footnotes provide the basis for our calculations within different habitats and the rationale for the mud conversion rates employed. Also shown are subsequent estimates of the % contribution of fish carbonates to total carbonate mud production in each habitat type.

Analysis of fine sediment fractions from the sedimentary environments of Eleuthera Bank.

In order to undertake a preliminary investigation into whether similar crystallites to those produced by fish could be identified with the sedimentary environments on the Eleuthera Bank, we collected surficial sediment samples from a wide range of different habitats including; low energy protected embayment sites, coastal inlets with fringing mangroves, seagrass beds, patch reefs, open sands with sparse algal cover, and from sites at 15 m depth on the main reef (Fig. S1). Following collection, samples were wet sieved through a 63 μm sieve, with the material passing through the sieve being retained and allowed to settle out in large glass vessels. Samples were then subject to triplicate distilled water rinses to remove extraneous salts, before drying in a low temperature (40 ˚C) oven, and storage in glass vials. Subsequently, this mud-grade carbonate fraction was fully resuspended in distilled water and allowed to settle out for between 1.5 and 2 hours, after which time a proportion of the waters above the settled sediment where removed with a pipette and transferred onto silicon plates (approx 2 cm^2) that had previously been mounted onto SEM stubs. This process was undertaken in order to isolate the very finest (< ~10 μm) sediment fraction within which our previous observations indicated most fish crystals were likely to occur. Samples were then allowed to dry in a low temperature (40 ˚C) oven and then examined using the same SEM procedures described above (Section 2.1). All samples contained crystallites that were morphologically identical to those observed to be produced by fish held in the laboratory. Representative examples are shown in Supplementary Fig. 17.
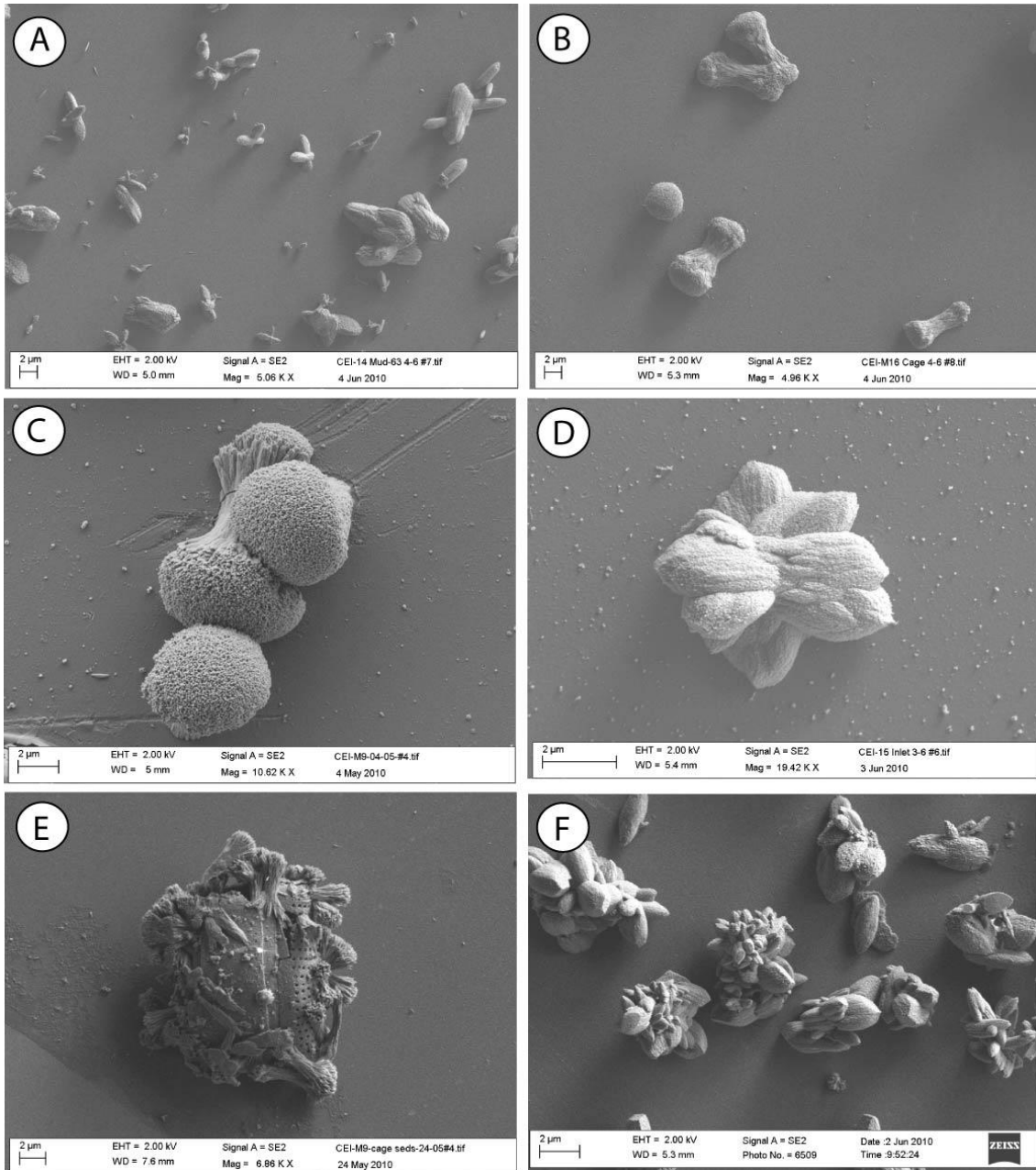
Supplementary Figure 17. Crystallites in the fine-sediment fractions from a range of modern environments across the Eleuthera Bank, Bahamas. (A) Individual and discrete clusters of ellipsoidal crystallites from muddy low energy embaymensites; (B) Discrete dumbbell morphology crystallites from reefal environments (15 m water depth); (C) Close up of dumbbell morphology crystallites from from reefal environments (15 m water depth); (D) Cluster of ellipsoidal morphology crystallites from shallow mangrove-fringed coastal inlet site; (E) Dumbbell and ellipsoidal morphology crystallites coating the surface of a fragmented foraminifera test from reefal environments (15 m water depth); (F) Multiple aggregates of ellipsoidal cystallites from shallow seagrass bed environments.

Additional references

34. Randall, J.E. (1967) Food habitats of reef fishes of the West Indies. *Stud Trop Oceanogr.* **5**, 665-847.

35. Froese, R., Pauly. D. (2010) World Wide Web electronic publication: www.fishbase.org.

36. Harborne, A.R. *et al.* (2008) Tropical coastal habitats as surrogates of fish community structure, grazing, and fisheries value. *Ecol Appl* **18**, 1689-1701.

37. Dravis, J. (1979) Rapid and widespread generation of recent oolitic hardgrounds on a high energy Bahamian platform, Eleuthera Bank, Bahamas. *J. Sed. Petrol.*, **49**, 195-208.

38. Gaffey, S.J. & Bronniman, C.E. (1993) Effects of bleaching on organic and mineral phases in biogenic carbonates *J. Sed. Petrol.,* **63**, 752-754.

39. Hardy, R. & Tucker, M. (1988) *Techniques in Sedimentology* 191-228 (Blackwell Scientific Publications).

40. Mackenzie*, F.T. et al.* (1983) Magnesian calcites: Low-temperature occurrence, solubility and solid-solution behavior. *Rev. Mineral. Geochem. 11, 97–144.*

41. Bischoff, W.D., Bishop, F.C. & Mackenzie, F.T. (1983) Biogenically produced magnesian calcite: inhomogeneities in chemical and physical properties: comparison with synthetic phases. *Am. Mineral.* **68**, 1183-1188.

42. Bischoff, W.D., Sharma, S.K. & Mackenzie, F.T. (1985) Carbonate ion disorder in synthetic and biogenic magnesian calcites: a Raman spectral study *Am. Mineral.* **70**, 581-589.

43. Milliman, J.D., Gastner, M. & Muller, J. (1971) Utilization of magnesium in coralline algae*. Geol. Soc. Am. Bull.* **82**, 573-580.

44. Goldsmith, J.R., Graf, D.L. & Heard, H.C. (1961) Lattice constants of the calcium-magnesium carbonates. *Am. Mineral.* **46**, 453-459.

45. Hills, A.G. (1973) *Acid– Base Balance; Chemistry, Physiology, Pathophysiology* (Williams and Wilkins, Baltimore, USA) 381 pp.

46. Clarke, A. & Johnston, N.M. (1999) Scaling of metabolic rate with body mass and temperature in teleost fish. *J. Anim. Ecol.*, **68**, 893-905.

47. Genz J, Taylor JR, Grosell M. (2008) Effects of salinity on intestinal bicarbonate secretion and compensatory regulation of acid-base balance in *Opsanus beta*. *J Exp Biol* **211**, 2327-2335.

48. Grosell, M., Nielsen, C. and Bianchini, A. (2002) Sodium turnover rate determines sensitivity to acute copper and silver exposure in freshwater animals. *Comparative Biochemistry and Physiology Part C: Toxicology & Pharmacology* **133**, 287-303.

49. Green, E.P., Mumby, P.J., Edwards, A.J. & Clark, C.D. (2000) *Remote sensing handbook for tropical coastal management* (Coastal Management Sourcebooks 3, UNESCO).

50. Mumby, P.J., Clark, C.D., Green, E.P. & Edwards, A.J. (1998) Benefits of water column correction and contextual editing for mapping coral reefs. *Int J Remote Sens.* **19**, 203-210.

51. Mumby, P.J. & Harborne, A.R. (1999) Development of a systematic classification scheme of marine habitats to facilitate regional management and mapping of Caribbean coral reefs. *Biol Conserv* **88**,155-163.

52. Mumby P.J. *et al.* (2004) Mangroves enhance the biomass of coral reef fish communities in the Caribbean. *Nature* **427**, 533-536.

53. Bohnsack, J.A. & Harper, D.E. (1988) *Length-weight relationships of selected marine reef fishes from the southeastern United States and the Caribbean.* (NOAA Technical Memorandum NMFS-SEFC-215).

54. Willis, T.J. (2001) Visual census methods underestimate density and diversity of cryptic reef fishes. *J Fish Biol* **59**,1408-1411.

55. Smith-Vaniz W.F., Jelks, H.L. & Rocha, L.A. (2006) Relevance of cryptic fishes in biodiversity assessments: A case study at Buck Island Reef National Monument, St. Croix. *Bull Mar Sci* **79**, 17-48.

56. Land, L.S. (1970) Carbonate mud; production by epibiont growth on *Thalassia testudinum. J Sed. Pet.* **40**, 1361-1363.

57. Nelsen, J.E. & Ginsburg, R.N. (1986) Calcium carbonate production by epibionts on *Thalassia* in Florida Bay *J Sed. Pet.* **56**, 622-628.

58. Frankovich, T.A. & Zieman, J.C. (1994) Total epiphyte and epiphytic carbonate production on *Thalassia testudinum* across Florida Bay. *Bull. Mar. Sci.* **54**, 679-695.

59. Stockman, K.W., Ginsburg, R.N. & Shinn, E.A. (1967) The production of lime mud by algae in South Florida *J Sed. Pet.* **37**, 633-648.

60. Neumann, A. C. & Land, L.S. (1975) Lime mud deposition and calcareous algae in the Bight of Abaco, Bahamas: a budget *J Sed. Pet.* **45**, 763-786.

61. Multer, H.G. (1988) Growth rate, ultrastructure and sediment contribution of *Halimeda incrassata* and *Halimeda monile*, Nonsuch and Falmouth Bays, Antigua, W.I. *Coral Reefs* 6, 179-186.

62. Bosence, D. (1989) Biogenic carbonate production in Florida Bay *Bull. Mar. Sci.* **44**, 419-433.

63. Rützler, K. (1975) The role of burrowing sponges in bioerosion. *Oecologia*. **19**, 203-216.

64. Fütterer, D.K. (1974) Significance of the boring sponge *Cliona* for the origin of fine grained material of carbonate sediments *J. Sed. Pet.* **44**, 79-84.